Defense Nuclear Agency
Alexandria, VA 22310-3398

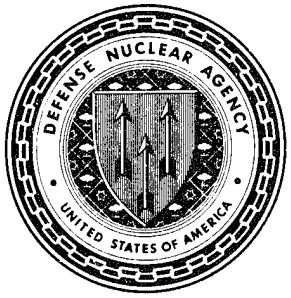

DNA-TR-95-32

Equation of State of Clay, Shale, and Slate

William W. Anderson
Yusheng Zhao
Thomas J. Ahrens
California Institute of Technology
Seismological Laboratory
1201 E. California Blvd.
Pasadena, CA 91125

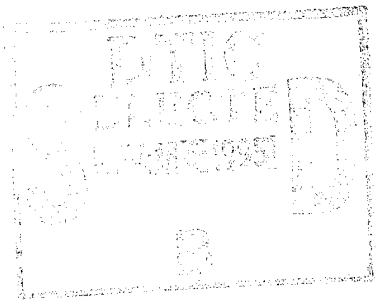

November 1995

Technical Report

CONTRACT No. DNA 001-92-C-0128

Approved for public release;
distribution is unlimited.

DESTRUCTION NOTICE:

Destroy this report when it is no longer needed.
Do not return to sender.

PLEASE NOTIFY THE DEFENSE NUCLEAR AGENCY, ATTN: CSTI, 6801TELEGRAPH ROAD, ALEXANDRIA, VA 22310-3398, IF YOUR ADDRESS IS INCORRECT, IF YOU WISH IT DELETED FROM THE DISTRIBUTION LIST, OR IF THE ADDRESSEE IS NO LONGER EMPLOYED BY YOUR ORGANIZATION.

DISTRIBUTION LIST UPDATE

This mailer is provided to enable DNA to maintain current distribution lists for reports. (We would appreciate your providing the requested information.)

☐ Add the individual listed to your distribution list.

☐ Delete the cited organization/individual.

☐ Change of address.

NOTE:
Please return the mailing label from the document so that any additions, changes, corrections or deletions can be made easily. For distribution cancellation or more information call DNA/IMAS (703) 325-1036.

NAME: _____

ORGANIZATION: _____

OLD ADDRESS	CURRENT ADDRESS
_____	_____
_____	_____
_____	_____

TELEPHONE NUMBER: ( ) _____

DNA PUBLICATION NUMBER/TITLE	CHANGES/DELETIONS/ADDITIONS, etc.) *(Attach Sheet if more Space is Required)*
_____	_____
_____	_____
_____	_____

DNA OR OTHER GOVERNMENT CONTRACT NUMBER: _____

CERTIFICATION OF NEED-TO-KNOW BY GOVERNMENT SPONSOR (if other than DNA):

SPONSORING ORGANIZATION: _____

CONTRACTING OFFICER OR REPRESENTATIVE: _____

SIGNATURE: _____

CUT HERE AND RETURN

REPORT DOCUMENTATION PAGE

Form Approved
OMB No. 0704-0188

1. AGENCY USE ONLY (Leave blank)	2. REPORT DATE	3. REPORT TYPE AND DATES COVERED
	951101	Technical 920930 – 950430

4. TITLE AND SUBTITLE

Equation of State of Clay, Shale, and Slate

5. FUNDING NUMBERS

C - DNA 001-92-C-0128
PE - 63711H
PR - AE
TA - CE
WU- DH920128

6. AUTHOR(S)

William W. Anderson, Yusheng Zhao, and Thomas J. Ahrens

7. PERFORMING ORGANIZATION NAME(S) AND ADDRESS(ES)

California Institute of Technology
Seismological Laboratory
1201 E. California Blvd.
Pasadena, CA 91125

8. PERFORMING ORGANIZATION REPORT NUMBER

9. SPONSORING/MONITORING AGENCY NAME(S) AND ADDRESS(ES)

Defense Nuclear Agency
6801 Telegraph Road
Alexandria, VA 22310-3398
FCTTS/Martinez

10. SPONSORING/MONITORING AGENCY REPORT NUMBER

DNA-TR-95-32

11. SUPPLEMENTARY NOTES

This work was sponsored by the Defense Nuclear Agency under RDT&E RMC Code B4613D AE CE 60008 5900A 25904D.

12a. DISTRIBUTION/AVAILABILITY STATEMENT

Approved for public release; distribution is unlimited.

12b. DISTRIBUTION CODE

13. ABSTRACT *(Maximum 200 words)*

New shock compression and release adiabat data to ~150 GPa are reported for kaolinite clay and rocks derived from clay- and mica-rich materials. The kaolinite data yield an STP isentropic bulk modulus (K_{so}) of 49.4 GPa. This is very similar to K_{so} for muscovite mica (52 GPa), although the density is lower (2.594 Mg/m^3 vs. 2.835 Mg/m^3 for muscovite). Unlike muscovite, kaolinite apparently transforms to a new (unidentified) phase under shock compression. Carbonate-poor shale (~ 8% $CaCO_3$ by weight) is less compressible (K_{so} = 61.1 GPa) than a carbonate-rich (~33% $CaCO_3$ by weight) shale (K_{so} = 30.9 GPa). This appears to be the result of the clay/mica ratio and the presence of zeolitic water in the carbonate-rich shale rather than carbonate content. The compressibility of slate (K_{so} = 50.5 GPa) is very similar to that of carbonate-poor shale at low pressures. All of these rocks transform to high-pressure phase assemblages, with marked increases in density (r = 3.359, 3.659, 3.740, and 4.110 Mg/m^3 for kaolinite, carbonate-rich and carbonate-poor shales, and slate, respectively, at P = 0), on shock compression. The behavior of this high pressure phase material is strongly influenced by the abundance of H_2O in the rock. Release adiabat data show conversion of high- to low-density material in kaolinite and shales upon release, but not in slate.

14. SUBJECT TERMS

Clay
Shock Waves
Equation-of-State
Slate
Shale

15. NUMBER OF PAGES

58

16. PRICE CODE

17. SECURITY CLASSIFICATION OF REPORT	18. SECURITY CLASSIFICATION OF THIS PAGE	19. SECURITY CLASSIFICATION OF ABSTRACT	20. LIMITATION OF ABSTRACT
UNCLASSIFIED	UNCLASSIFIED	UNCLASSIFIED	SAR

NSN 7540-280-5500

Standard Form 298 (Rev.2-89)
Prescribed by ANSI Sts. 239-18
298-102

CLASSIFIED BY:

N/A since Unclassified.

DECLASSIFY ON:

N/A since Unclassified.

SUMMARY

Table 9 summarizes the equation of state and mixed-phase regime parameters for kaolinite clay and the pelitic rocks examined in this study. Examination of the data in light of the compositions of the rocks suggests that the low pressure properties of pelitic rocks are dominated by the relative fractions of clays and micas, as well as the presence of zeolitic water in open crystal structures. The effect of the clay/mica ratio is primarily on the density, as clays are less dense than micas, but have bulk moduli very similar to those of micas. Zeolitic water has a significant effect on both the density and the bulk modulus of the rocks in their low pressure phases.

The high pressure portions of the Hugoniots represent states in which the minerals in the rocks have transformed to high pressure polymorphs. Models of the high pressure behavior, obtained by considering the mixing of the high pressure phases of the individual minerals, results in Hugoniot states that are more dense than the experimentally measured states. This suggests that the current equation of state of one or more phases common to all three rock types is in error. The high pressure phase density seems to be correlated with the H_2O content of the rock, with high density rocks having lower water contents. properties are affected mostly by the abundance of minerals containing no volatiles, relative to clays and carbonates.

The use of a constant specific heat in the equation of state models allows easy calculation of the release adiabats. Comparison with the release adiabat data shows that both kaolinite and calcareous shale high pressure phases convert to a lower density material upon release from the shock state. Slate, however, may retain the high pressure phase to very low pressures. The hysteresis in the shock-release path, and thus the fraction of shock energy deposited, can be calculated using these release adiabats. Because of formation of low-density material upon release, the calculated energy deposition will be greater than the actual value. Incorporation of such information into models, along with suitable models for the low-pressure behavior, will allow the decay of a shock wave resulting from irreversible heating to be calculated.

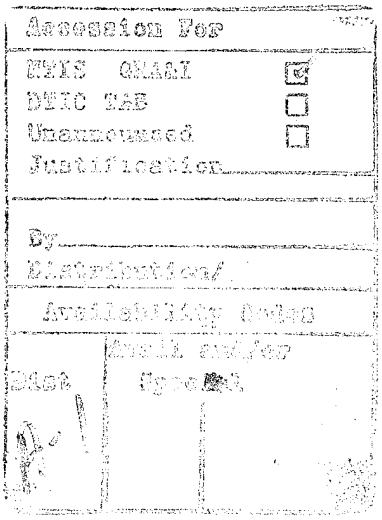

PREFACE

Work performed for the Test Science and Technology Office (FCTT), Field Command Defense Nuclear Agency (FCDNA) under Contract No. DNA001-92-C-0128. The Contracting Officer's Technical Representative (COTR) was Audrey A. Martinez.
This program was directed by Professor Thomas J. Ahrens. Detailed experiments were conducted by Drs. William W. Anderson and Yusheng Zhao. Professor Ahrens and Dr. Anderson prepared the Final Report. Technical review for FCDNA was performed by Audrey A. Martinez (FCTTS) and Dr. Eric Rinehart (FCTT-T). Dr. George Baladi was the Assistant Director for FCTT, COL. Harlan A. Lawson was the Director, Test Operations Directorate (FCT), and COL Darrell W. Singleton was the Commander, FCDNA.

CONVERSION TABLE

Conversion factors for U.S. Customary to metric (SI) units of measurement.

MULTIPLY → / ← TO GET	BY → / ← BY	TO GET → / ← DIVIDE
angstrom	1.000 000 X E -10	meters (m)
atmosphere (normal)	1.013 25 X E +2	kilo pascal (kPa)
bar	1.000 000 X E +2	kilo pascal (kPa)
barn	1.000 000 X E -28	meter^2 (m^2)
British thermal unit (thermochemical)	1.054 350 X E +3	joule (J)
calorie (thermochemical)	4.184 000	joule (J)
cal (thermochemical/cm^2)	4.184 000 X E -2	mega joule/m^2 (MJ/m^2)
curie	3.700 000 X E +1	*giga becquerel (GBq)
degree (angle)	1.745 329 X E -2	radian (rad)
degree Fahrenheit	$t_k = (t^oF + 459.67)/1.8$	degree kelvin (K)
electron volt	1.602 19 X E -19	joule (J)
erg	1.000 000 X E -7	joule (J)
erg/second	1.000 000 X E -7	watt (W)
foot	3.048 000 X E -1	meter (m)
foot-pound-force	1.355 818	joule (J)
gallon (U.S. liquid)	3.785 412 X E -3	meter^3 (m^3)
inch	2.540 000 X E -2	meter (m)
jerk	1.000 000 X E +9	joule (J)
joule/kilogram (J/kg) radiation dose absorbed	1.000 000	Gray (Gy)
kilotons	4.183	terajoules
kip (1000 lbf)	4.448 222 X E +3	newton (N)
kip/inch^2 (ksi)	6.894 757 X E +3	kilo pascal (kPa)
ktap	1.000 000 X E +2	newton-second/m^2 ($N\text{-}s/m^2$)
micron	1.000 000 X E -6	meter (m)
mil	2.540 000 X E -5	meter (m)
mile (international)	1.609 344 X E +3	meter (m)
ounce	2.834 952 X E -2	kilogram (kg)
pound-force (lbs avoirdupois)	4.448 222	newton (N)
pound-force inch	1.129 848 X E -1	newton-meter (N·m)
pound-force/inch	1.751 268 X E +2	newton/meter (N/m)
pound-force/foot^2	4.788 026 X E -2	kilo pascal (kPa)
pound-force/inch^2 (psi)	6.894 757	kilo pascal (kPa)
pound-mass (lbm avoirdupois)	4.535 924 X E -1	kilogram (kg)
pound-mass-foot^2 (moment of inertia)	4.214 011 X E -2	kilogram-meter^2 ($kg\cdot m^2$)
pound-mass/foot^3	1.601 846 X E +1	kilogram/meter^3 (kg/m^3)
rad (radiation dose absorbed)	1.000 000 X E -2	**Gray (Gy)
roentgen	2.579 760 X E -4	coulomb/kilogram (C/kg)
shake	1.000 000 X E -8	second (s)
slug	1.459 390 X E +1	kilogram (kg)
torr (mm Hg, 0^o C)	1.333 22 X E -1	kilo pascal (kPa)

*The becquerel (Bq) is the SI unit of radioactivity; 1 Bq = 1 event/s.
**The Gray (GY) is the SI unit of absorbed radiation.

TABLE OF CONTENTS

FIGURES

TABLES

SECTION 1
INTRODUCTION

Clays, shales and slates make up a series of genetically related sedimentary and metamorphic rocks, called pelitic rocks, characterized by high contents of hydrous aluminosilicate minerals. Pelitic rocks form an abundant class of materials found at and near the earth's surface in a wide range of geologic environments. Essentially all ancient sedimentary basins now contain shales or slates and many modern basins contain unconsolidated clay mixtures which will, over geologic time, become shales and perhaps slates. Because pelitic rocks are so widespread, making up ~30% of all sediments and meta-sediments, accurate knowledge of their behavior under shock compression and adiabatic release is essential for the modelling of shock-producing events, such as impacts and explosions, in sedimentary and metamorphic terranes.

In this study, we conduct an experimental investigation of the shock and release behavior of a clay (kaolinite), a shale, and a slate, and combine our experimental results with previously reported data for similar materials to develop equations of state (EOS) of clays and pelitic rocks. We also address the ability to predict the equation of state of pelitic rocks from a knowledge of the composition. The equation of state of kaolinite is expected to be very similar in most respects to those of other clay minerals. The kaolinite EOS is compared to that of muscovite mica to examine the consequences of conversion of clays to micas during metamorphism of shales into slates.

We also use the equations of state and experimental data to study the shock-release path hysteresis and consequent energy deposition in pelitic materials. Knowledge of such behavior allows us to draw conclusions about the decay rate of shock waves expanding from an impact or confined explosion.

SECTION 2
GENETIC RELATIONSHIPS BETWEEN CLAYS, SHALES, AND SLATES

Clays are part of a class of hydrous aluminosilicate minerals called phyllosilicates, characterized by sheets of silica and aluminum hydroxide separated by layers of cations. Clays, admixed with other minerals (notably quartz, SiO_2), form the starting material for formation of shales and slates. Shales are sedimentary rocks formed by the physical deposition of clay minerals with very fine grains of other minerals and subsequent compaction and cementation. The cementing material most often is organic material formed from detrital remains of organisms or carbonate minerals (usually calcite, $CaCO_3$) deposited by chemical precipitation. As such, the properties of shales can be modelled as a mixture of clay, other detrital minerals, and the relevant cementing material. One complication in the terminology is that "clay" is both a mineralogical and a textural term, denoting either a member of the clay group of phyllosilicate minerals or any sediment that is very fine-grained. The primary complication is that the prominent layering in shales can introduce anisotropy to the wave propagation behavior.

Slates result from relatively low-grade metamorphism of shales. The most common metamorphic reaction is the conversion of clays to micas with the evolution of water. Continued metamorphism to higher grades results in the production of phyllites, which are very similar to slates but have experienced textural coarsening due to recrystallization of minerals, schists, in which grain growth has become extreme for micas, and gneisses, which represent extreme metamorphism, just short of wholesale melting of the rock.

SECTION 3
EXPERIMENTAL TECHNIQUES

3.1 SAMPLES AND PREPARATION.

Pure kaolinite (no detectable contaminants in X-ray diffraction analysis) from Georgia was obtained from a major rock and mineral sample supplier. These specimens were compact but unconsolidated and contained negligible contaminants. The material was disaggregated in a mortar and pestle, moistened with deionized water, and pressed in a special die under a pressure of ~1 kbar into pellets 37 mm in diameter and 4-5 mm thick. The pellets had densities in the range of 1.93-2.16 Mg/m^3.

A calcareous shale was collected, by us, for this study. It was obtained from the lower Chambless Limestone (Cambrian) in the southernmost Marble Mountains of the central Mojave Desert in California. Volatile-free oxide composition was determined via inductively-coupled plasma mass spectroscopy and X-ray fluorescence spectrometry. CO_2 in carbonates was determined by reaction with acid and volumetric measurement of gas evolved. The composition is given in Table 3-1. The samples had a mean nonporous (crystal) density of 2.615 Mg/m^3. Ultrasonic measurements of longitudinal and transverse wave velocities give $V_p = 4.505$ km/s and $V_s = 2.753$ km/s, respectively.

Slate samples were obtained from Portland, Maine, and the vicinity of Slatedale, Pennsylvania. Both slates have similar properties, with an average bulk density of 2.756 Mg/m^3. The Pennsylvania slate has been studied previously [Furnish, 1992; Davies and Smith, 1994] and its mineralogical composition is reported by Davies and Smith [1994]. They also give ultrasonic elastic wave velocities for this slate as $V_p = 4.08$ km/s and $V_s =$ 2.19 km/s.

3.2 EXPERIMENTAL PROCEDURE.

The experimental techniques for this study are discussed in detail elsewhere [Ahrens, 1987]. The surfaces of a rectangular sample approximately 1.3 cm wide, 1.5 cm long, and 3-4 mm thick, were ground flat and parallel. In contrast, the kaolinite samples were first reduced to a powder and cold pressed in a die. Flatness and parallelism was achieved to within ±0.02 mm. The sample was then mounted on a metal driver plate (Figure 1) with standard buffers and/or inclined mirrors placed on the free (rear) surface of the sample.

Shock arrival mirrors were placed against the rear surfaces of the driver plate, sample, and buffers. During the experiment, the driver plate was impacted by a gun-launched projectile containing a metal impactor (flyer plate). The impact generated a planar shock wave which propagates through the driver plate, sample, and buffer materials. Arrival of the shock wave at the free surface of each component

Table 3-1. Oxide composition analyses of calcareous shale from Marble Mountains, central Mojave Desert, California.

Oxide	Weight % (ICP)[a]	Weight % (XRF)[b]
SiO_2	44.59	44.20
TiO_2	0.84	0.76
Al_2O_3	9.68	9.42
Fe_2O_3	4.77	4.73
CaO	19.09	19.30
MgO	1.33	1.39
Na_2O	0.33	0.13
K_2O	2.04	2.25
CO_2[c]	14.34	14.34
H_2O[d]	4.21	3.46
Total	100.94	99.98

(a) Inductively-couple plasma source emission spectrometry

(b) X-ray fluorescence spectrometry

(c) Determined by gas evolution on treatment with acid.

(d) Determined by thermal desorption and decomposition (different samples).

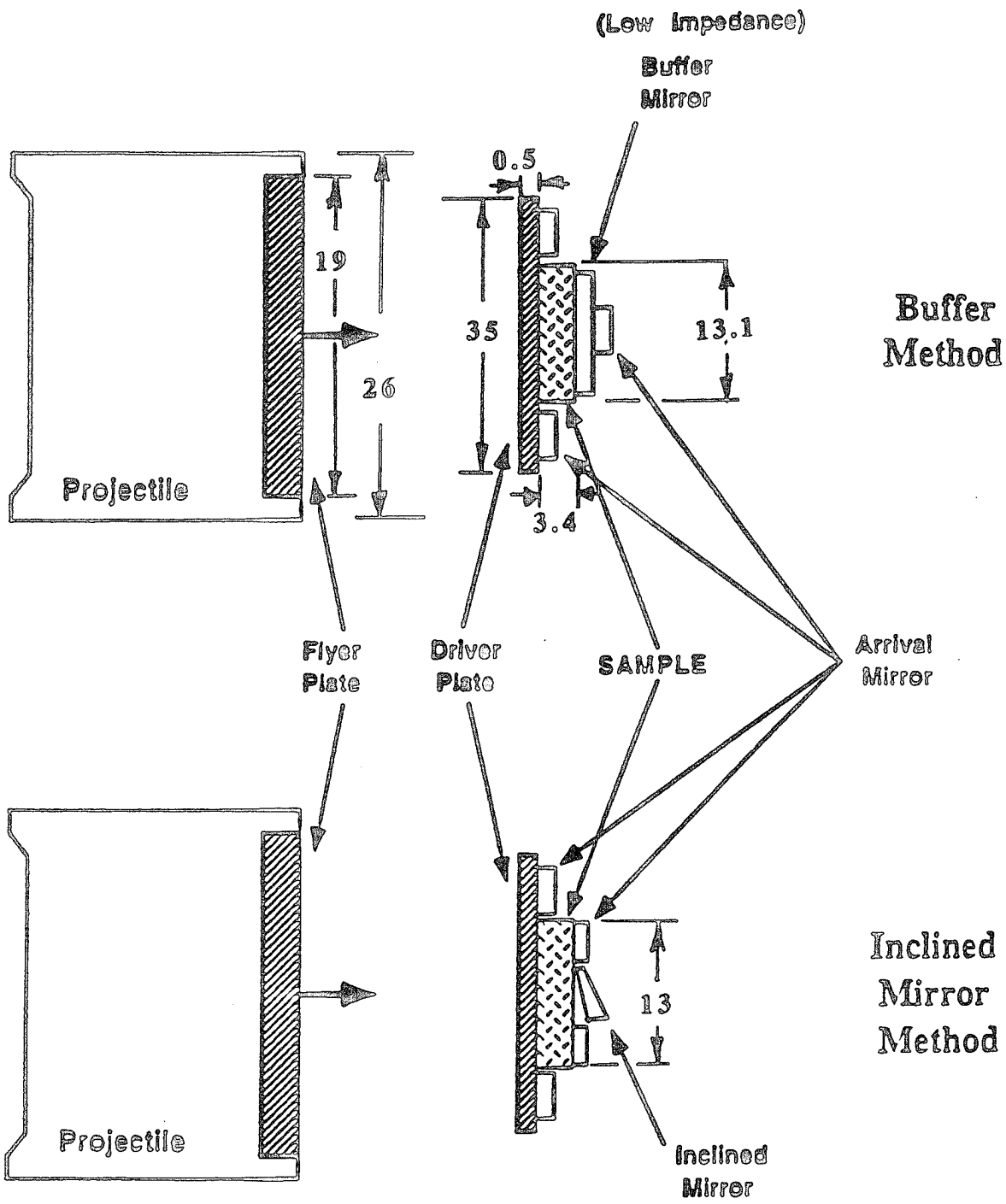

Figure 3-1. Experimental arrangement for shock wave equation of state experiments. All mirrors 1 mm thick. Dimensions in mm.

caused disruption of the specular reflection from the shock arrival mirrors. One spatial dimension of the target, including all shock arrival mirrors, was imaged as a function of time by a streak camera, allowing the shock wave transit times, and thus the shock wave velocities through the target components of known thickness, to be determined. The internal energy E, pressure P, density ρ, and particle velocity u_p of the shocked sample and buffer are constrained from the conservation of mass, energy and momentum and the requirement that pressure within the two materials must remain in contact requires that particle velocity be continuous across material interfaces.

The buffers and inclined mirrors are used to measure points on the release adiabats of the samples by the requirement that the P-u_p condition in the released state of the sample be identical with that of the shocked buffer or the free surface in the case of the inclined mirror. Table 3-2 gives the properties of the materials used for flyer and driver plates and buffers in this study.

The shock Hugoniot of a material, which is the locus of final states achieved by shock compression, can be conveniently described as a polynomial representation of the shock wave velocity, U_s in terms of the particle velocity, u_p:

$$U_s = C_0 + su_p + s'u_p^{\,2} + \ldots \tag{3.1}$$

Here Co is the intercept for zero particle velocity and is $d\,V_s/d\,U_p$. For simple non-transforming media, Co is the zero pressure bulk sound velocity and $S = [(d\,K_{0S}/dP)_{P=0} + 1]/4$ where K_{0S} is the zero pressure isentropic bulk modulus. The polynomial may be truncated at first or second order (if material phase are not apparent). The pressure, P, density, r, and internal energy, E, in the shocked state are given by

$$P_H = P_0 + \rho_{00} U_s u_p \tag{3.2}$$

$$\rho_H = \rho_{00} \frac{U_s}{U_s - u_p} \tag{3.3}$$

$$E_H = E_{00} + \frac{1}{2}(P_H + P_0)(V_{00} - V_H) = E_{00} + \frac{1}{2}u_p^{\,2} \tag{3.4}$$

Here, the subscripts 0 and H refer to the unshocked and shocked (Hugoniot) states, respectively, and the subscript 00 denotes the possibility that the initial sample may be porous or may be in a different thermodynamic phase from that in the final shock state. Here V is equal to $1/\rho$, where the same subscripts apply. P_0 is usually negligible compared to P_H and is thus set to zero, while E_{00} is arbitrary and so we also set $E_{00} = 0$ as the initial condition.

Table 3-2. Shock Hugoniot parameters for standard materials used in this study.

Material	ρ_0 (Mg/m3)	C_0 (km/s)	s	s' (s/km)	Source
Aluminum - 1100	2.707	5.386	1.339		1
Aluminum - 2024	2.784	5.330	1.34		2
Tungsten	19.224	4.029	1.237		1
Tantalum	16.650	3.293	1.308		2
Lexan	1.193	2.449	1.498		3
		4.817	0.589		4
		1.907	1.431		5
Polystyrene	0.0474	0.362	0.9165	0.04982	6

(1) Marsh [1980]
(2) Mitchell and Nellis [1981]
(3) Fit to data from Marsh [1980] for $u_p \leq 2.605 \text{km/s}$.
(4) Fit to data from Marsh [1980] for $2.605 \text{km/s} < u_p \leq 3.456 \text{km/s}$.
(5) Fit to data from Marsh [1980] for $u_p \geq 3.456 \text{km/s}$.
(6) Calculated from ρ_{00} using expression from Anderson and Ahrens [1993]

3.3 EXPERIMENTAL RESULTS

3.3.1 Kaolinite.

Table 3-3 and Figure 3-2 present the experimental results for kaolinite. The tabulated densities of the release states are obtained using the Reimann integral formalism and approximating the release adiabats as straight line segments in the P-V plane [Lyzenga and Ahrens, 1978]. The U_s-u_p projection of the data (Figure 3-2a) show a discontinuity suggestive of a phase change, although it is also possible that this discontinuity may be the result of variability between samples. We fit the three segments of the U_s-u_p Hugoniot with $C_0 = 0.820$ km/s and $s = 2.26$ for $u_p < 1.821$ km/s, $C_0 = 4.589$ km/s and $s = 0.19$ for $1.821 \leq u_p < 2.219$ km/s, and $C_0 = 1.497$ km/s and $s = 1.59$ for $u_p \geq 2.219$ km/s. The data of Sekine et al. [1991] for muscovite (Figure 3-3a) show a similar structure, although they interpret their data as showing no phase transformation under shock compression. The P-V projection of the kaolinite data (Figure 3-2b) show a sudden steepening at higher shock pressures, which is strongly indicative of a phase change. In contrast to the U_s-u_p data, the P-V data for muscovite (Figure 3-3a) show no significant structure. As some clay minerals have crystal structures and chemical formulae similar to those of muscovite, these data taken together suggest that the presence or absence of a shock-induced phase transition in clay minerals depends on the details of the composition and structure. Kikuchi et al. [1993] suggested that kaolinite and smectic clays do undergo phase transformation, possibly with the formation of a melt or amorphous material, at shock pressures of ~30 GPa. The other possibility is that, in kaolinite, we are observing a transformation related to the strong heating in the samples, which are ~20-25% porous. The muscovite samples studied by Sekine et al. [1991] were nonporous and therefore not heated as strongly. Based on the sum of the evidence available, we suggest that relatively H_2O-rich clays undergo partial devolatilization, with the liberated H_2O acting as a flux for the formation of a water-rich melt, under the proper P-T conditions. Here T is absolute temperature in Kelvins. The composition of this melt and the P-T regime under which this reaction is favored cannot be determined from the presently available data.

3.3.2 Shale.

Table 3-4 and Figure 3-4 present our results for calcareous shale. The U_s-u_p data can be broken down into three regions and fit by Equation (3.1) truncated to first order. The fit

parameters are C_0 = 3.803±0.097 km/s and s = 1.463±0.115 for u_p < 1.12 km/s, C_0 = 4.853±0.115 km/s and s = 0.523±0.073 for 1.12 ≤ u_p < 1.98 km/s, and C_0 = 2.405±0.139 km/s and s = 1.761±0.054 for u_p ≥ 1.98 km/s. The high compressibility

Table 3-3. Experimental Data for Kaolinite.

Shot	Flyer/ Driver	Impact Velocity (km/s)	Sample Density (Mg/m^3)	Particle Velocity (km/s)	Shock Velocity (km/s)	Pressure (GPa)	Density (Mg/m^3)	Particle Velocity (km/s)	Pressure (GPa)	Density (Mg/m^3)
967	Al2024	0.918 (.007)	1.932	0.707 (.006)	2.417 (.013)	3.30 (0.04)	2.730 (.025)			
968	W	1.245 (.013)	1.932	1.149 (.012)	3.423 (.016)	7.60 (0.11)	2.908 (.030)	1.307 (.064)	6.87 (.46) (Lexan Buffer)	2.646 (.661)
937	W	2.03 (.02)	2.113	4.94 (.06)	1.80 (0.03)	18.8 (0.4)	3.33 >06)	2.21 (.03)	15.2 (.4) (Lexan Buffer)	2.88 (.05)
969	W	2.502 (.019)	1.946	2.240 (.017)	5.019 (.029)	21.88 (0.25)	3.516 (.036)	2.555 (.081)	19.13 (.95) (Lexan Buffer)	3.121 (.421)
273	Al1101	4.85 (.02)	2.137	2.96 (.09)	6.24 (.07)	39.5 (2.6)	4.06 (.09)	3.17 (.09)	27.2 (.9) (Lexan Buffer)	4.00 (.08)
								4.71 (.09)	1.29 (.04) (Polystyrene Foam Buffer)	3.06 (.06)
272	Ta	4.90 (.02)	2.160	3.96 (.09)	8.37 (.09)	71.5 (1.2)	4.10 (.09)	4.48 (.08)	49.0 (.9) (Lexan Buffer)	3.90 (.07)
								6.33 (.09)	2.45 (.09) (Polystyrene Foam Buffer)	3.07 (.05)
290	Ta	6.046 (.007)	1.916	4.945 (.010)	9.162 (.059)	86.83 (.72)	4.164 (.044)	5.325 (.087)	60.52 (1.75) (Lexan Buffer)	4.071 (.069)

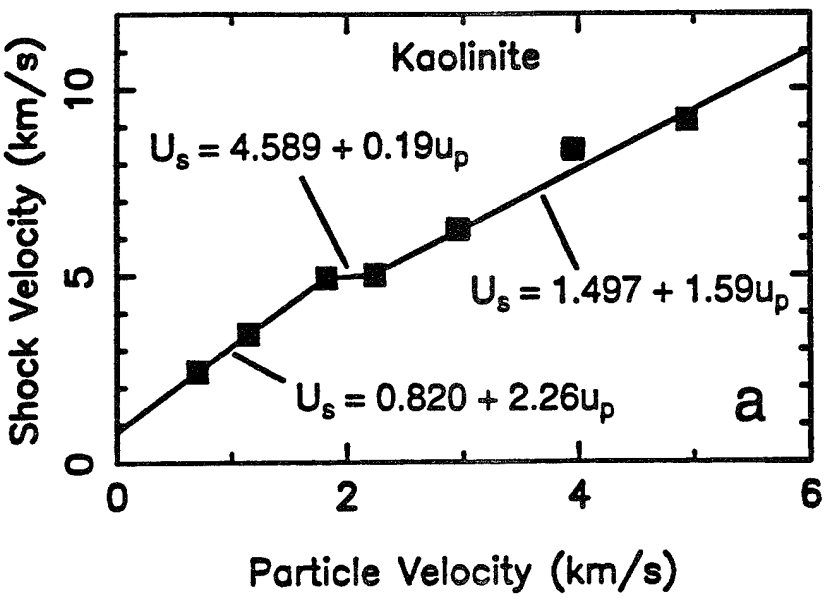

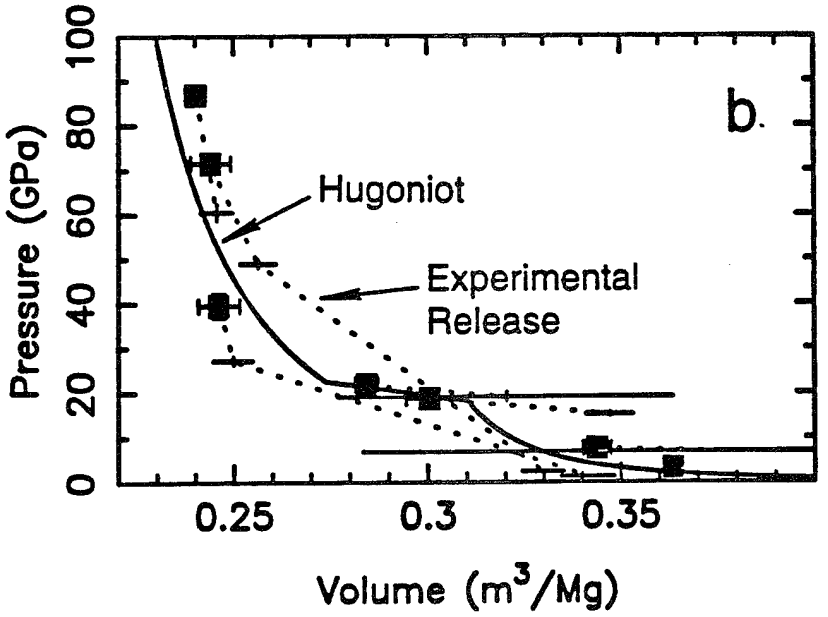

Figure 3-2. Experimental data for kaolinite: (a) U_s-u_p projection with empirical fits to the data; (b) P-V projection of data and Hugoniot calculated from U_s-u_p fit.

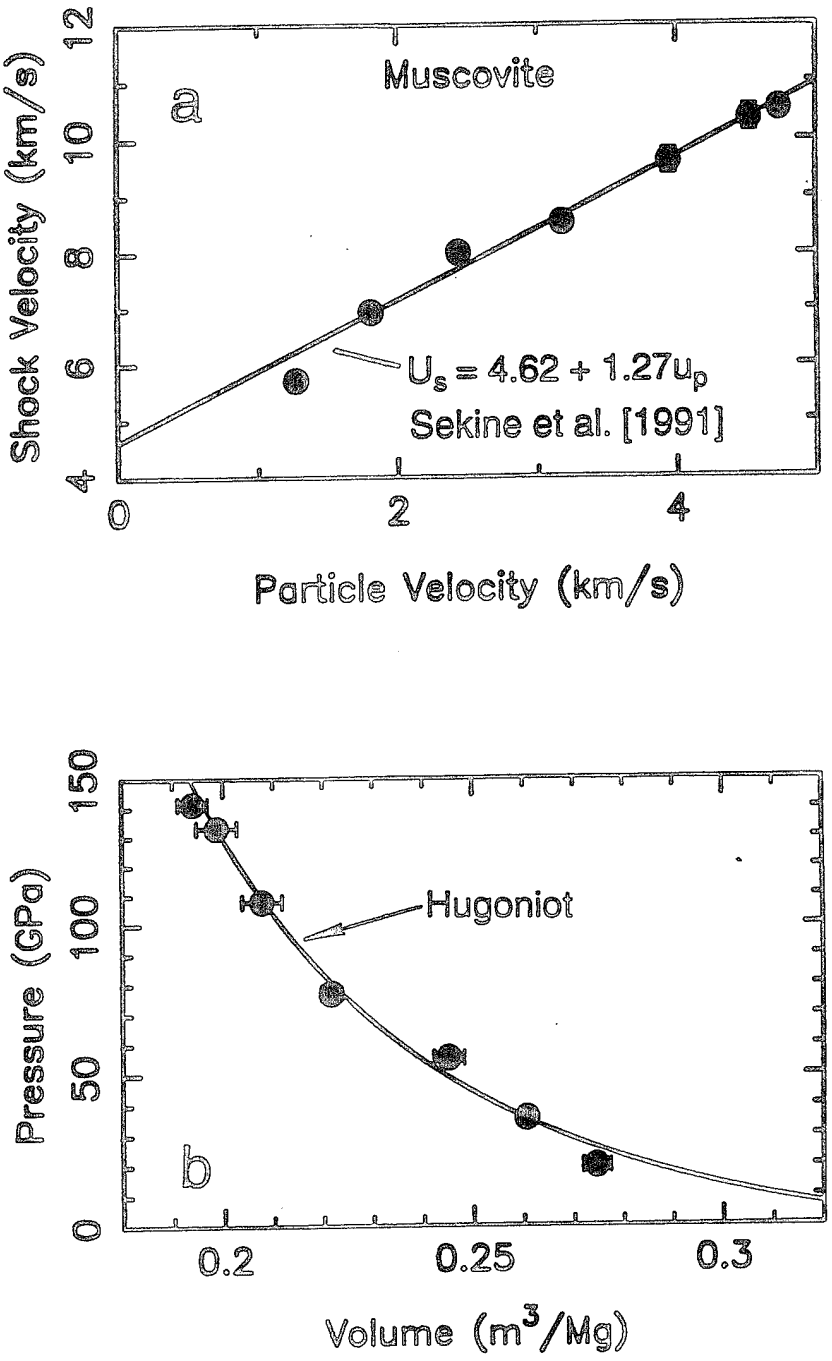

Figure 3-3. Experimental data for muscovite from Sekine et al. [1992]: (a) U_s-u_p projection with empirical fit to the data from Sekine et al [1991]; (b) P-V projection of data and Hugoniot calculated from U_s-u_p fit.

Table 3-4. Experimental Data for Calcareous Shale.

Shot	Flyer/ Driver	Impact Velocity (km/s)	Sample Density (Mg/m^3)	Particle Velocity (km/s)	Shock Velocity (km/s)	Pressure (GPa)	Density (Mg/m^3)	Particle Velocity (km/s)	Pressure (GPa)	Density (Mg/m^3)
933	Al 2024	0.64 (0.01)	2.580	0.18[a] (0.02)	4.62[a] (0.09)	2.2[a] (0.2)	2.69[a] (0.07)			
				0.39[b] (0.03)	3.19[b] (0.04)	3.9[b] (0.2)	2.89[b] (0.08)	0.75 (0.07)	0	2.64 (0.06)
									Free Surface	
904	Al 2024	0.84 (0.02)	2.582	0.20[a] (0.02)	4.87[a] (0.09)	2.5[a] (0.2)	2.69[a] (0.07)			
				0.48[b] (0.02)	4.54[b] (0.05)	5.8[b] (0.2)	2.88[b] (0.07)	0.92 (0.05)	0	2.63 (0.05)
									Free Surface	
920	Al 2024	1.05 (.01)	2.566	0.60 (0.04)	4.62 (0.23)	7.1 (0.5)	2.95 (0.18)		VISAR	
912	Al 2024	1.44 (0.02)	2.574	0.84 (0.02)	4.76 (0.09)	10.3 (0.3)	3.13 (0.09)	1.17 (0.03)	5.9 (0.2)	2.90 (0.4)
									Lexan Buffer	
								1.64 (0.09)	0	2.62 (0.06)
									Free Surface	
918	Al 2024	1.82 (0.01)	2.556	1.01 (0.04)	5.31 (0.15)	13.9 (0.5)	3.19 (0.11)		VISAR	
902	W	1.26 (0.02)	2.571	1.08 (0.02)	5.43 (0.05)	15.1 (0.4)	3.21 (0.04)	1.60 (0.02)	9.2 (0.3)	2.80 (0.03)
									Lexan Buffer	
919	Al 2024	2.50 (0.01)	2.580	1.40 (0.04)	5.58 (0.12)	20.0 (0.6)	3.41 (0.10)		VISAR	

Table 3-4. Experimental data for calcareous shale.(Continued)

Shot	Flyer/ Driver	Impact Velocity (km/s)	Sample Density (Mg/m^3)	Particle Velocity (km/s)	Shock Velocity (km/s)	Pressure (GPa)	Density (Mg/m^3)	Particle Velocity (km/s)	Pressure (GPa)	Density (Mg/m^3)
901	W	2.29 (0.02)	2.573	1.96 (0.03)	5.87 (0.06)	29.5 (0.5)	3.86 (0.06)	2.63 (0.03)	20.0 (0.3)	.327 (0.04)
									Lexan Buffer	
903	W	2.49 (0.02)	2.582	2.11 (0.04)	5.98 (0.09)	32.6 (0.8)	3.99 (0.06)	2.73 (0.01)	21.2 (0.9)	3.53 (0.07)
									Lexan Buffer	
263	Al 1100/ Al 2024	5.02 (0.02)	2.579	2.72 (0.09)	7.30 (0.08)	51.4 (2.1)	4.13 (0.09)	3.27 (0.08)	28.7 (0.9)	3.91 (0.07)
									Lexan Buffer	
								4.73 (0.09)	1.3 (0.1)	3.00 (0.05)
									Polystyrene Foam Buffer	
260	Ta	4.95 (0.02)	2.589	3.81 (0.05)	9.16 (0.12)	90.4 (0.9)	4.44 (0.09)	4.68 (0.02)	52.8 (0.9)	4.07 (0.07)
									Lexan Buffer	
								6.62 (0.03)	2.71 (0.19)	3.12 (0.05)
									Polystryene Foam Buffer	
265	Ta	6.13 (0.02)	2.582	4.67 (0.07)	10.40 (0.20)	125.6 (2.6)	4.67 (0.09)	5.62 (0.02)	73.0 (0.9)	4.33 (0.09)
									Lexan Buffer	
								7.28 (0.02)	3.34 (0.14)	3.70 (0.07)
									Polystyrene Foam Buffer	

[a]Elastic wave.
[b]Plastic wave.

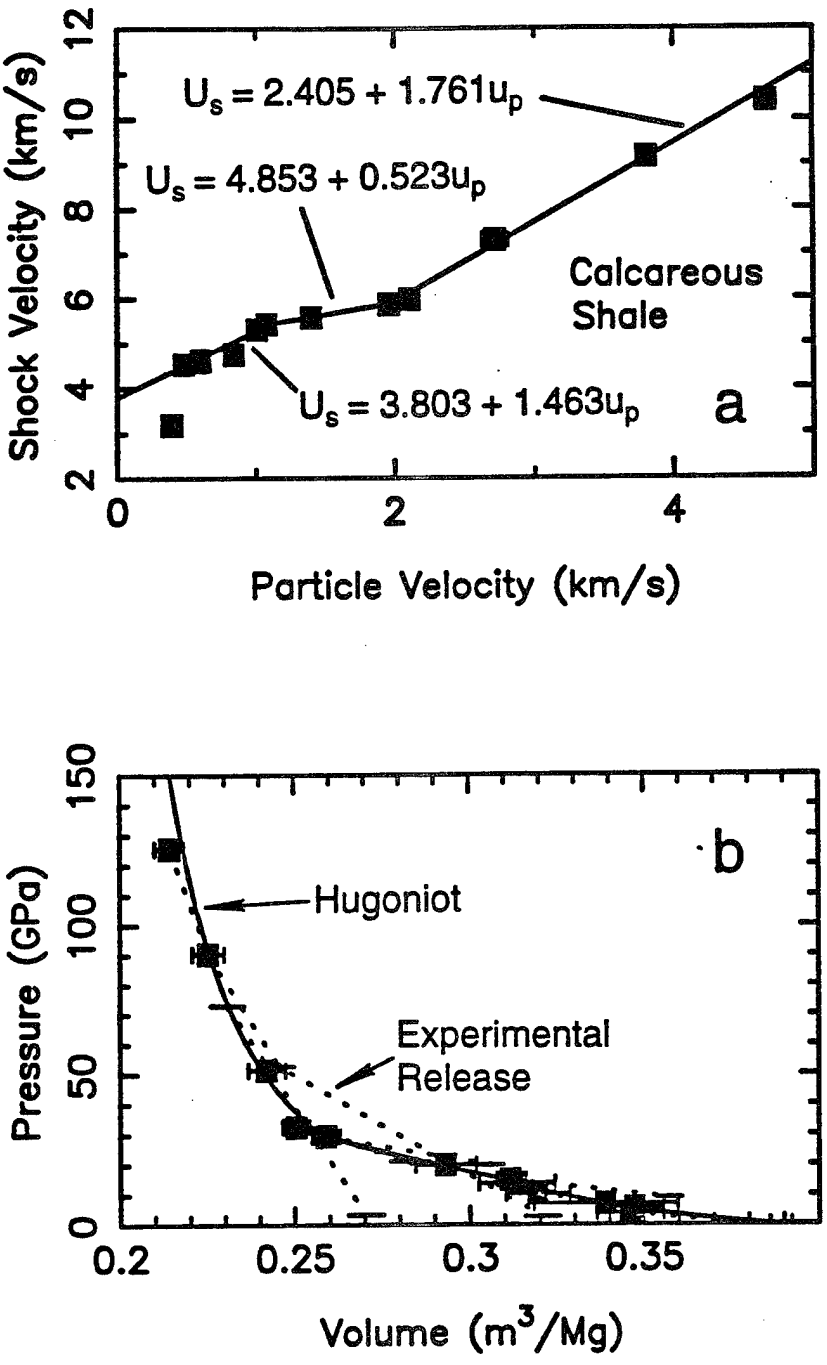

Figure 3-4. Experimental data for calcareous shale: (a) U_s-u_p projection with empirical fits to the data; (b) P-V projection of data and Hugoniot calculated from U_s-u_p fit.

shown at low pressures in the P-V data and the definitely defined segments of the U_s-u_p Hugoniot suggest that the lowest pressure data represent Hugoniot states entirely within the low-pressure phase of the shale and the highest pressure data represent states entirely within a high pressure phase. The intervening region represents a mixed-phase regime where the formation of the high pressure phase is incomplete, so that the Hugoniot states fall on a mixing line between the metastable extensions of the low and high pressure phase Hugoniot curves. We should note here that the term "phase" is not strictly correct, since the rock is a mixture of several different mineral phases. Rather, the term "low pressure phase" in the present context is used to refer to a material composed of the same mineral phases as the original sample, whereas the term "high pressure phase" refers to a material in which some or all of the constituent minerals have transformed to high pressure polymorphs. The term "mixed phase" in the present paper refers to a material in which minerals have partially transformed to high pressure polymorphs, but the transformation is incomplete.

In the lowest pressure experiments, the plastic shock wave in the shale was preceded by an elastic precursor. If we assume that the velocity U_{el} of elastic precursor should be identical to V_p under infinitesimal strain, then the elastic precursor obeys $U_{el} = 4.505 + 1.2u_p$ for U_{el} and u_p in km/s.

3.3.3 Slate.

Table 3-5 and Figure 3-5 give the present data for slate. The two slates studied are very similar, with the slate from Maine being slightly more dense. The experimental data for the two rocks are statistically indistinguishable, so we have chosen to combine the two into a single data set. The same Pennsylvania slate as used in the present experiments has been studied by Davies and Smith [1994] and Furnish [1992]. To increase the number of data available and thus the quality of the results, we have combined those experimental results with the present data. They are also presented in Figure 3-5.

The U_s-u_p data for slate, as for the calcareous shale, can be divided into three regions characterized by straight line segments. The parameters for these are $C_0 = 4.203$ km/s and $s = 2.837$ for $u_p < 0.286$ km/s, $C_0 = 4.795$ km/s and $s = 0.768$ for $0.286 \leq u_p < 2.169$ km/s, and $C_0 = 3.220$ km/s and $s = 1.494$ for $u_p \geq 2.169$km/s, for $\rho_{00} = 2.756$ Mg/m^3. As with the shale data, we interpret the structure in the slate Hugoniot as indicating the existence of single "phase" regions at high and low pressures, with an intervening mixed-

phase region characterized by partial transformation of the low to the high pressure phase.

Table 3-5. Experimental Data for Slate.

Shot	Flyer/ Driver	Impact Velocity (km/s)	Sample Density (Mg/m^3)	Particle Velocity (km/s)	Shock Velocity (km/s)	Pressure (GPa)	Density (Mg/m^3)	Particle Velocity (km/s)	Pressure (GPa)	Density (Mg/m^3)
963	Al2024	0.848 (.008)	2.784 (.003)	0.147[a] (.003)	5.880[a] (.069)	2.40[a] (.06)	2.856[a] (.004)			
				0.443[b] (.006)	5.145[b] (.062)	6.62[b] (.09)	3.035[b] (.001)	0.798 (.016)	0 (Free Surface)	2.869 (.012)
962	W	2.015 (.017)	2.788 (.003)	1.675 (.015)	6.239 (.025)	29.13 (.27)	3.811 (.014)	2.285 (.047)	16.01 (.46) (Lexan Buffer)	3.439 (.074)
								2.853 (.025)	0.46 (.03) (Polystyrene Foam Buffer)	3.210 (.075)
282	Al1101	4.841 (.006)	2.790 (.002)	2.570 (.0110	7.225 (.047)	51.81 (.27)	4.331 (.023)	3.397 (.350)	27.63 (2.92) (Lexan Buffer)	3.859 (.347)
								4.181 (.088)	1.00 (.08) (Polystyrene Foam Buffer)	3.543 (.353)
281	Al1101	5.014 (.008)	2.734 (.002)	2.703 (.011)	7.182 (.031)	53.07 (.24)	4.384 (.019)	3.133 (.330)	24.91 (2.66) (Lexan Buffer)	4.251 (.138)
								4.478 (.063)	1.16 (.08) (Polystyrene Foam Buffer)	3.218 (.550)
276	Ta	5.016 (.007)	2.787 (.004)	3.831 (.010)	9.052 (.070)	96.63 (.64)	4.831 (.034)	5.119 (.079)	56.37 (1.52) (Lexan Buffer)	4.029 (.125)
								6.276 (.092)	2.49 (.18) (Polystyrene Foam Buffer)	3.604 (.125)

Table 3-5. Experimental data for slate.(Continued)

Shot	Flyer/ Driver	Impact Velocity (km/s)	Sample Density (Mg/m^3)	Particle Velocity (km/s)	Shock Velocity (km/s)	Pressure (GPa)	Density (Mg/m^3)	Particle Velocity (km/s)	Pressure (GPa)	Density (Mg/m^3)
280	Ta	5.922 (.007)	2.736 (.003)	4.498 (.031)	9.925 (.351)	122.13 (3.49)	5.003 (.163)	6.094 (.074)	77.26 (1.65)	3.897 (.272)
									(Lexan Buffer)	
								7.220 (.065)	3.28 (.20)	3.653 (.242)
									(Polystyrene Foam Buffer)	
283	Ta	6.669 (.007)	2.787 (.002)	5.016 (.011)	10.734 (.053)	150.06 (.66)	5.232 (.028)	6.416 (.051)	84.88 (1.12)	4.521 (.068)
									(Lexan Buffer)	
								7.971 (.069)	4.09 (.25)	2.982 (.076)
									(Polystyrene Foam Buffer)	

[a]Elastc wave.
[b]Plastic wave

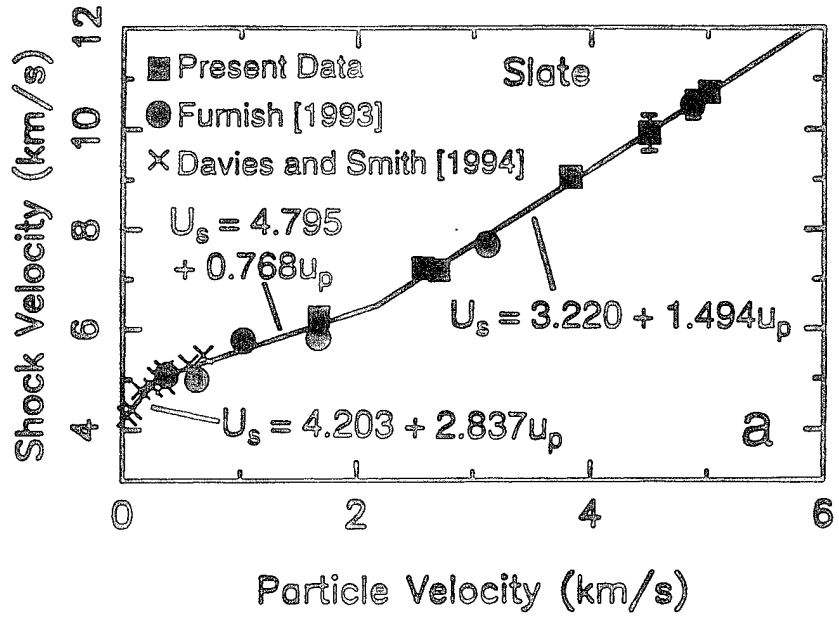

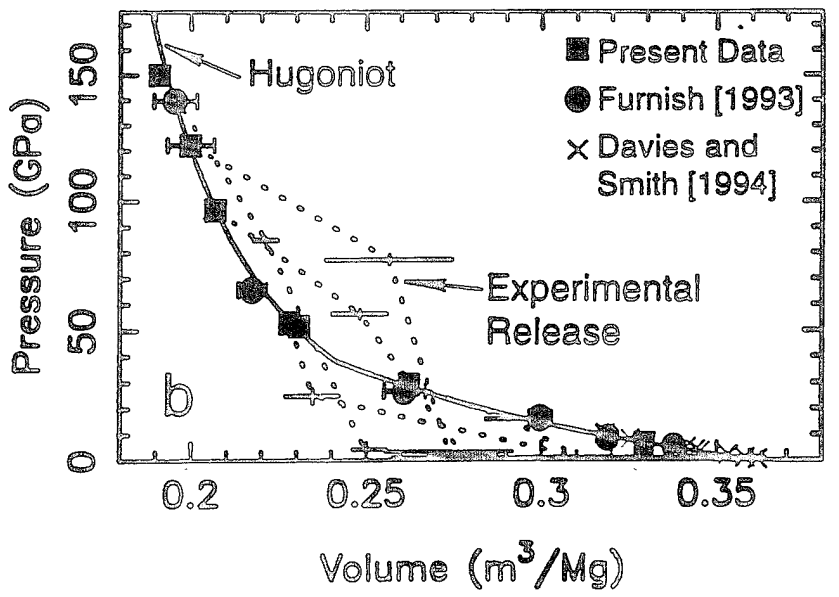

Figure 3-5. Experimental data for slate: (a) U_s-u_p projection with empirical fits to the data; (b) P-V projection of data and Hugoniot calculated from U_s-u_p fit.

We detected an elastic precursor to the plastic shock in our lowest-velocity shot (Figure 3-6), indicating that material strength is significant at low shock stresses. Davies and Smith [1994] also state that their data show evidence of an elastic precursor to the plastic shock wave at low pressures. This suggests that the low-velocity segment of the U_s-u_p Hugoniot presented above is representative of the elastic wave, rather than the plastic wave. Support for this conclusion can be found in the fact that the intercept of the low velocity segment is close to the measured longitudinal wave velocity of 4.08 km/s [Davies and Smith, 1994]. If the Hugoniot represented a purely plastic wave, the intercept should be the bulk sound velocity of 3.27 km/s.

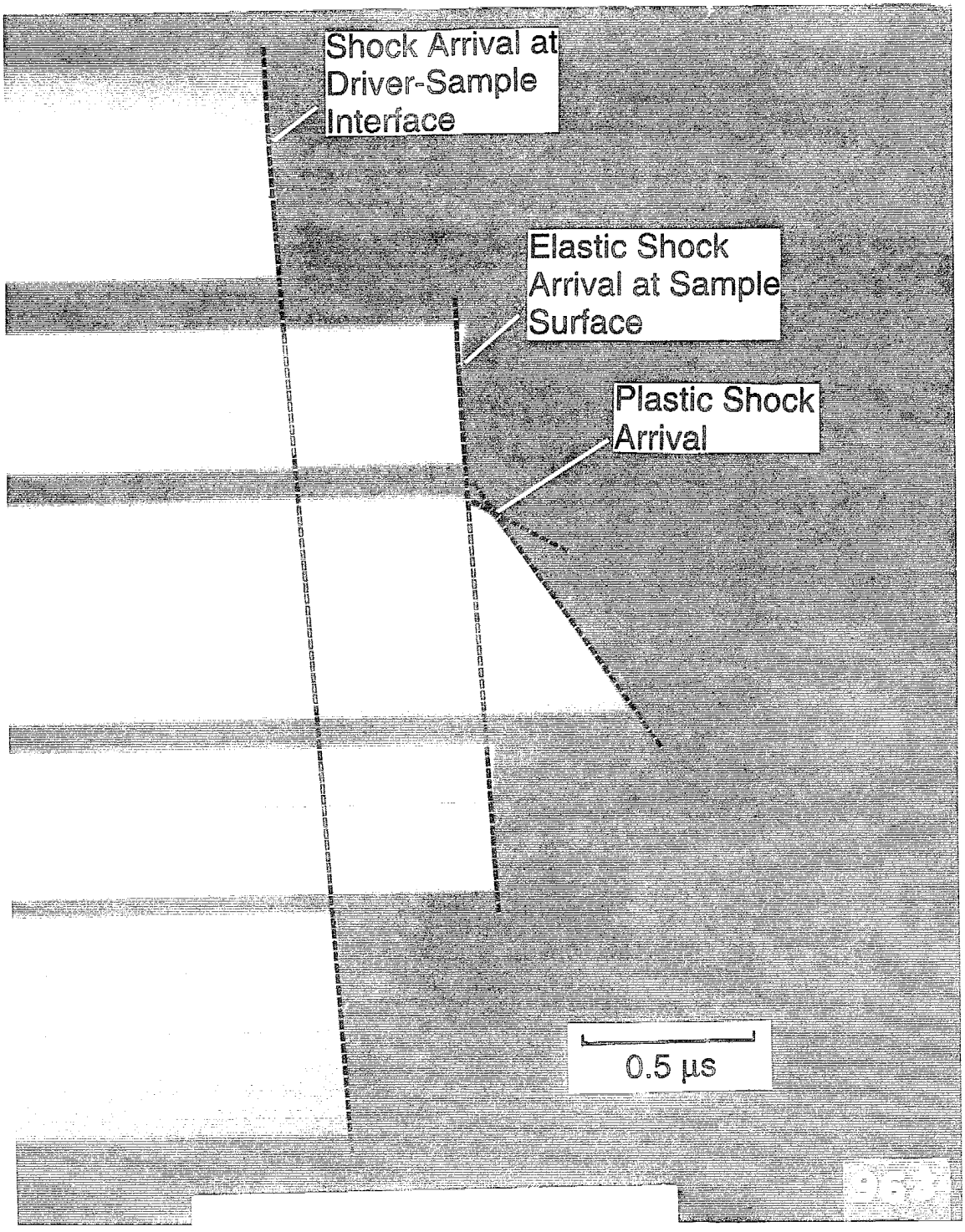

Figure 3-6. Streak record from shot 963 showing arrival of elastic and plastic shock waves at the free surface of the sample.

SECTION 4
EQUATIONS OF STATE

4.1 KAOLINITE.

While the experimental U_s-u_p data are useful, they are valid only for the initial bulk density of the samples on which the experiments were performed. In the case of kaolinite, this is only 75-80% of the theoretical bulk density of the material. In order to extrapolate the data to other densities, we require an appropriate general thermodynamic equation of state for each phase or mixture of phases. These are obtained by fitting the *P-V* Hugoniot data in each single phase region of the Hugoniot. The pressure P_H on the Hugoniot can be related to the pressure and energy on an isentrope of the same phase at the same density by

$$P_H = \frac{E_S - \frac{V_H}{\gamma_H} P_S + E_{tr}}{\frac{V_{00} - V_H}{2} - \frac{V_H}{\gamma_H}} \tag{4.1}$$

where P_S is the pressure on the isentrope at specific volume V_H, E_S is the internal energy gained by compression to volume V_H from some reference condition (usually 1 bar and 298 K) along the isentrope, γ is the thermodynamic Grüneisen parameter, and E_{tr} is the internal energy difference between the Hugoniot phase at that reference condition and the initial state of the sample. For the present discussion, we will always use 1 bar and 298 K as the reference conditions for the isentrope.

There are a number of parameterizations that can be used for the reference isentrope. We have chosen to use the 3rd order Birch-Murnaghan equation of state (BMEOS) because it has been shown to provide a good description of geologic materials and is widely used. With the BMEOS, P_S and E_S are given by [Ahrens, 1979]:

$$P_S = \frac{3}{2} K_{0S} \left(x^7 - x^5\right)\left(1 + \xi - \xi x^2\right) \tag{4.2}$$

$$E_S = -\int_{V_0}^{V_H} P_S dV = \frac{9}{2} V_0 K_{0S} \left[\frac{x^4}{4} - \frac{x^2}{2} + \frac{1}{4} - \xi\left(\frac{x^6}{6} - \frac{x^4}{4} + \frac{x^2}{2} - \frac{1}{6}\right)\right] \tag{4.3}$$

where

$$x = \left(\frac{V_0}{V}\right)^{1/3} \tag{4.4}$$

and

$$\xi = \frac{3}{4}(4 - K') \tag{4.5}$$

where ρ_0 is the density, $V_0 = 1/\rho_0$, and K_{0S} and K' are the isentropic bulk modulus and its pressure derivative, all at the reference condition. The Grüneisen parameter is usually expressed in the form

$$\gamma = \gamma_0 \left(\frac{V}{V_0}\right)^n \tag{4.6}$$

For the present study, we have fit the EOS parameters to the experimental data using a nonlinear least squares fit directly to Equations 4.1-4.6. The value of ρ_0 for the low pressure phase is set to the density based on the crystallographic parameters of kaolinite. The value we use is obtained from the molar mass and volume stated by Robie et al. [1978]. Because we have only a few data, we have chosen to assume $\gamma_0 = 1$ and $n = 1$, since the fit is insensitive to the values of these parameters and the assumed values are typical for most materials. The fit values of K_{0S} and K' for the low pressure phase are 49.4 GPa and 2.36, respectively.

For the high pressure phase, we again assume $\gamma_0 = 1$ and $n = 1$. We also assume $E_{tr} = 0.5$ MJ/kg, which is in the middle of the range of values displayed by the high pressure phases of silicate minerals. We also used the second order (in strain) BMEOS (see Ahrens [1987]), in which $\xi = 0$ (i.e., $K' = 4$), then $P_S = K_{0S}\ (X^7 - X^5)/2$. Under these assumptions, the fit gives $\rho_0 = 3.359$ Mg/m^3 and $K_{0S} = 157$ GPa.

4.2 PELITIC ROCKS.

As much as possible, we have tried to make use of supplemental data to constrain the values of parameters that are only weakly dependent on fits to the shock wave data or when

the number of available data are limited. We use measured Archimedian densities for the values of ρ_0 of the low pressure phases. We also use compositional data to estimate some properties. By determining the mineral abundances in the rocks, we can use simple rules to obtain several important EOS parameters. The assumption we make is that the process of physical mixing without chemical reactions or phase changes conserves the total volume of material. Under this assumption, we can get density, bulk modulus, and thermal expansion coefficient via

$$\rho_0 = \left(\sum_i m_i V_{0i} \right)^{-1} \tag{4.7}$$

$$K_0 = \rho_0 \left(\sum_i \frac{m_i}{\rho_{0i} K_{0i}} \right)^{-1} \tag{4.8}$$

$$\alpha_0 = \rho_0 \sum_i \frac{m_i \alpha_{0i}}{\rho_{0i}} \tag{4.9}$$

where m is mass fraction, α is volume thermal expansion coefficient, and the subscript i refers the i'th mineral phase. Unsubscripted variables refer to the whole rock. Although we could use values of ρ_0 and K_{0S} from (4.7) and (4.8) as final EOS parameters, the fits to the shock wave data are very sensitive to these parameters and it is best to allow them to vary during the fitting process. Strictly speaking, (4.8) only refers to the isothermal bulk modulus, but the difference between the isothermal and isentropic bulk moduli at ambient conditions is negligible. We also note that energy is additive, so that specific heat and transition energy are given by

$$C_V = \sum_i m_i C_{Vi} \tag{4.10}$$

$$E_{tr} = \sum_i m_i E_{tri} \tag{4.11}$$

For the present investigation, we have assumed $C_V = 3R/\mu$, where μ is the mean atomic weight and R is the ideal gas constant. We can combine the values of ρ_0, K_{0S} α_0, and C_{V0} obtained from (4.7)-(4.10) to obtain γ_0 from

$$\gamma = \frac{\alpha K_S}{\rho C_P} \tag{4.12}$$

Note that, although the specific heat in (4.12) is C_P, not C_V, the distinction between these is negligible at ambient conditions, where γ_0 is defined. We also chose to estimate n by an average weighted by γ_0/ρ_0, under the assumption that this quantity is influenced most by phases with large volumes and large values of γ_0. In all the EOS fits, we have held γ_0, n, and E_{tr} at the values obtained by the prescriptions described above.

4.2.1 Equation of state of shale.

The shale we studied is relatively carbonate rich (32.6% $CaCO_3$ by weight). The carbonate content of shales can be quite variable, so we have concentrated here on a carbonate-rich shale and use published data for carbonate-poor shales to obtain two different equations of state. We used the composition (Table 3-1), on an H_2O-free basis, to calculate the equivalent mineral mixture model of the rock, and then accounted for H_2O in the analysis and corundum in the norm by converting feldspars and other minerals to clays and micas. We represent H_2O tied-up in the structure of clays and micas as a separate constituent. Table 4-1 gives the resulting approximate mineral composition. The rock is composed of roughly equal amounts of quartz, clays, and calcite. This result is confirmed by powder X-ray diffraction analysis. The mean Archimedian value for ρ_0 of the low pressure phase is 2.615 Mg/m^3, with calculated values of $\gamma_0 = 0.73$, $n = 1.52$, $C_V = 1396$ Jkg^{-1}K^{-1}. We held K_{0S} at 30.9 GPa, calculated from (4.8), and find that the fit to the low pressure data not affected by an elastic precursor gives $K' = 8.15$. The calculated parameters for the high pressure phase are $\gamma_0 = 1.2$, $n = 1.49$, $E_{tr} = .42$ MJ/kg, and $C_V = 1396$ Jkg^{-1}K^{-1}. A fit to the four highest pressure shock compression data gives $\rho_0 = 3.659$ Mg/m^3, $K_{0S} = 265$ GPa and $K' = 3.14$.

To study relatively carbonate-poor shales, we have combined the data of Trunin et al. [1988] and Al'tshuler and Pavlovskii [1971] for Russian shales and of Olinger [1978] for kerogen-free Chemung Shale. Trunin et al. [1988] give a chemical analysis of their shale, which we use as representative of all the samples, since the three data sets are the same within the scatter of the data. The analysis give ranges of abundances of different constituents, so that our estimation of the mineral content of the shales is only approximate. They also do not report an H_2O analysis but, based on the normative corundum abundance and the densities of the rocks, the dominant phyllosilicates are probably micas, rather than clays with the rock containing only ~8% $CaCO_3$. Table 4.2 gives the estimated mineral composition of these shales. We estimated ρ_0 for the low pressure phase on the

assumption that all the normative corundum was in muscovite and get $\rho_0 = 2.813$ Mg/m^3. Other calculated parameters are $\gamma_0 = 0.79$, $n = 1.73$, and $C_V = 1159$ Jkg^{-1}K^{-1}. To avoid possible problems caused by elastic precursors in the original data, we fit the low pressure phase EOS to the data in the pressure range from 10 GPa to 16 GPa and get $K_{0S} = 61.1$ GPa and $K' = 4.52$. Calculated parameters for the high pressure phase are $\gamma_0 = 0.93$, $n = 1.92$, $C_V = 1159$ Jkg^{-1}K^{-1}, and $E_{tr} = 0.62$ MJ/kg. A fit to data in the pressure range from

Table 4-1. Mineral composition of calcareous shale used in this study, estimated from oxide composition and X-ray diffraction analysis.

Mineral	Weight Percent
Quartz	32.1
Calcite	32.6
Clays and Micas	34.4
Zeolitic Water	1.1
Total	100.2

Table 4-2. Estimated mineral composition of carbonate-poor shale studied by Trunin et al. [1988].

Mineral	Weight Percent
Quartz	40
Plagioclase	15
Pyroxene	13
Calcite	8
Muscovite	20
Magnetite	4
Total	100

55 GPa to 120 GPa gives ρ_0 = 3.740 Mg/m^3, K_{0S}= 184 GPa and K' = 3.24.

4.2.2 Equation of state of slate.

Although we used slate from two separate locations, the total data set, including the scatter in the data, shows that the two are indistinguishable from the standpoint of their shock wave properties. The Pennsylvania slate used in this study has also been studied by Furnish [1992] and by Davies and Smith [1994]. Table 4-3 gives the mineral composition of the slate, as reported by Davies and Smith [1994] based on X-ray diffraction analysis. We assume that the material reported as amorphous in the analysis is actually clay minerals too disordered to give good X-ray diffraction peaks. Based on the densities and porosities reported by Furnish [1992], the value of ρ_0 for the low pressure phase is 2.823 Mg/m^3. Based on the mineral composition, we get K_{0S} = 50.5 GPa, γ_0 = 0.71, n = 1.65, and C_V= 1225 Jkg^{-1}K^{-1}. Most of the low pressure phase shock compression data are complicated by the presence of an elastic precursor, seen in our data and those of Davies and Smith [1994]. Based on the limited reliable data, K' = 8.0 for the low pressure phase. For the high pressure phase, we calculate γ_0 = 0.83, n = 1.8, C_V= 1225 Jkg^{-1}K^{-1}, and E_{tr} = 0.62 MJ/kg. A fit to the shock wave data above 50 GPa gives ρ_0 = 4.110 Mg/m^3, K_{0S}= 432 GPa and K' = 1.99.

Table 4-3. Mineralogy of Pennsylvania slate reported by Davies and Smith [1994].

Mineral	Weight Percent
Quartz	37
Plagioclase	12
Calcite	12
Ferroan Dolomite	7
Pyrite	3
Chlorite	8
Illite + Mica	16
Amorphous	5
Total	100

SECTION 5
DISCUSSION

5.1 MIXED-PHASE HUGONIOTS

A characteristic of the shock Hugoniot curves of most geologic materials seems to be the transformation of the material to a high pressure phase assemblage at shock pressures typically below 50 GPa. A complete description of the shock compression behavior of these materials requires that a suitable description be found for the behavior of this mixed phase region. We have taken the relatively simple assumption that the mixed-phase region between the low and high pressure phase regions can be modeled as a mixture of the Hugoniot states of the two phases. In particular, we use the same volume conservation prescription used earlier (Equation (4.7)) to estimate ρ_0, except that we now apply it to ρ_H at a given value of P_H:

$$\rho_H = \left[\frac{f_{HPP}}{\rho_{H,Hpp}} + \frac{1 - f_{HPP}}{\rho_{H,LPP}} \right]^{-1} \tag{5.1}$$

where f_{HPP} is the mass fraction of the high pressure phase. The starting state for both single phase Hugoniot curves must be the same. In reality, the prescription in (5.1) is only approximate, since the Hugoniot temperatures for the two phases at the same single-phase Hugoniot pressure are different, sometimes by the order of 10^3 K. However, since thermal expansion (α) is a relatively small effect, which become less significant with compression, made smaller by the decrease in a as α material is the effects of the temperature difference on the densities is much smaller than the density difference between the two phases.

In addition to the transformation from low pressure phases to high pressure phases, materials also eventually undergo melting as a result of shock-induced heating. Our data do not give clear evidence for this phenomenon. As we noted earlier, the "high pressure phase" of kaolinite may actually be a mixture of volatile-rich melt and volatile-depleted solid, based on previously reported results for samples which were shocked and then recovered. Unfortunately, such studies introduce an ambiguity as to when the melting actually occurs (i.e., upon compression or release). Previous work with silicate minerals that transform to high pressure phases, such as quartz, suggests that diaplectic glasses may form when a high pressure phase is kinetically inhibited from reverting to the low pressure phase upon release from the shocked state. The only clear evidence of a further phase

change, probably melting, as the shock pressure increases, is from the data of Trunin et al. [1988] for shale. Their highest pressure data (in the range from 199 to 450 GPa) show a different slope in the U_s-u_p plane from those of the lower pressure data we have used in this study. This break in slope probably indicates that these data are in either a mixed-phase region or in new single phase region of the Hugoniot.

To model the mixed-phase regions of the Hugoniots for the materials considered in this study, we have assumed that the transformation is kinetically inhibited, so that the transformation rate, and thus the fraction of material transformed, can be approximated by an Arrhenius relation of the form

$$f_{HPP} = A e^{-E_a/RT} \tag{5.2}$$

where E_a is an activation energy. We assume that some phase boundary must be crossed before any transformation takes place. Under the assumption that the rate-limiting temperature must be the preexisting phase, we use the Hugoniot temperature, T_H, of the low pressure phase. T_H is given by

$$T_H = T_0 \exp\left(-\int_{V_0}^{V_H} \frac{\gamma}{V} dV\right) + \frac{\gamma_H}{\rho_H C_V}(P_H - P_S) \tag{5.3}$$

where the first term is the temperature increase along the reference isentrope and the second term is the temperature increase associated with the entropy increase induced by the shock wave. As previously stated, we use T_0 = 298 K for all cases considered in this study.

For each material considered in this study, we fit the parameters of (5.3) to the value of f_{HPP}, obtained by finding the value that gives the proper density for each experimental point, and the calculated value of T_H for the low pressure phase. We assume that the kinetics are not dependent on the pressure, only on the temperature of the low pressure phase. This approach has obvious shortcomings, but insufficient data are available to develop a more rigorous thermodynamic model with phase boundaries, unless a fully thermodynamically consistent model, treating each mineral phase separately and accounting for temperature differences between the low and high pressure phases, is attempted. That is well beyond the scope of this study which examines whole-rock properties without the complications of considering each mineral species separately. We also are forced at the present to define the phase boundary between the low pressure phase and high pressure

phase as a constant pressure. While this must be in error, data for a range of different initial samples densities would be required to map out the *P-T* behavior of the boundaries. Above the boundary pressure, transformation to the high pressure phase is allowed, but not below.

Based on the present EOS results and the assumption of the Dulong-Petit limit for the specific heat, we get $A = 8$ and $E_a = 30.5$ kJ/mol for kaolinite, with the phase boundary at 12 GPa; $A = 7.8$ and $E_a = 15.8$ kJ/mol for the carbonate-poor shales, with the phase boundary at 17 GPa; $A = 58$ and $E_a = 28.6$ kJ/mol for the calcareous shale, with the phase boundary at 18 GPa; and $A = 1.34$ and $E_a = 5.26$ kJ/mol for slate, with the phase boundary at 21 GPa. Of course, the values of A allow the value of f_{HPP} to be greater than unity above a given temperature. Obviously, the value of f_{HPP} must be set equal to 1 for all cases when (19) would give $f_{HPP} > 1$. Figures 5-1--5-4 present the Hugoniot curves, obtained using the EOS parameters obtained in this study and the mixed phase region description presented here, in comparison to the experimental data.

5.2 COMPOSITIONAL TRENDS IN PROPERTIES.

One of the most pressing needs when considering the shock wave properties of geologic materials is to be able to use compositional and metamorphic history information to estimate parameters that would otherwise have required the performance of shock wave compression experiments. Part of the purpose of the present study is to use experimental data to draw conclusions concerning the effects of composition and metamorphism on the equations of state, so that trends could be identified.

We approach this problem in two ways. First, we can compare the high pressure region of the Hugoniot, calculated from the Hugoniots of the individual mineral constituents via the volume conservation prescription already presented (i.e., (11) but mixing Hugoniot volumes at a given pressure). These calculated curves are presented in Figures (5-2)-(5-4). The calculated curves underestimate the volume of the Hugoniot state. This suggests that the high pressure behavior of some constituent common to both shales and the slate is at present incorrectly described. It may also indicate that the amount and behavior of H_2O is are being improperly accounted for.

The second approach is to simply try to correlate trends in the fit EOS properties with trends in composition. The clearest trend is in the high-pressure phase value of ρ_0, which

increases with decreasing H_2O content. Although slate apparently does not follow the trend established by the other materials studied, we must remember that the lack of H_2O analyses for the carbonate-poor shale and the slate make estimates at to water content highly uncertain.

One of the most important conclusions to be drawn concerns the H_2O content of the rock. Pelitic rocks in which the dominant phyllosilicate minerals are micas (including chlorite for this discussion), tend to be more dense than those containing the more clays such as kaolinite, which contain more structural water. This can be traced directly to the

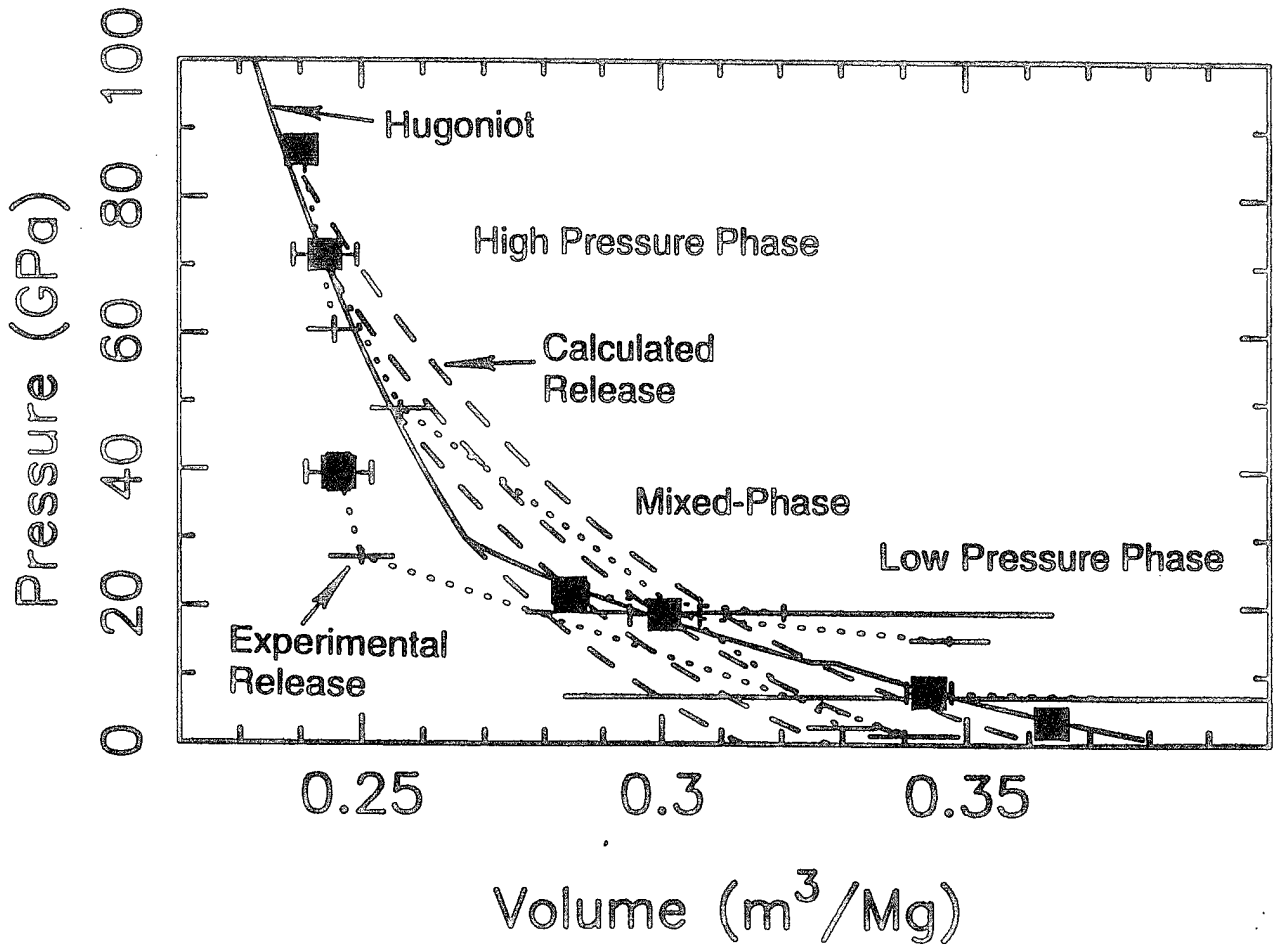

Figure 5-1. Hugoniot and release adiabats calculated for kaolinite from equation of state parameters with the mixed phase model connecting the low pressure phase and high pressure phase segments of the Hugoniot. The experimental data are also presented for comparison.

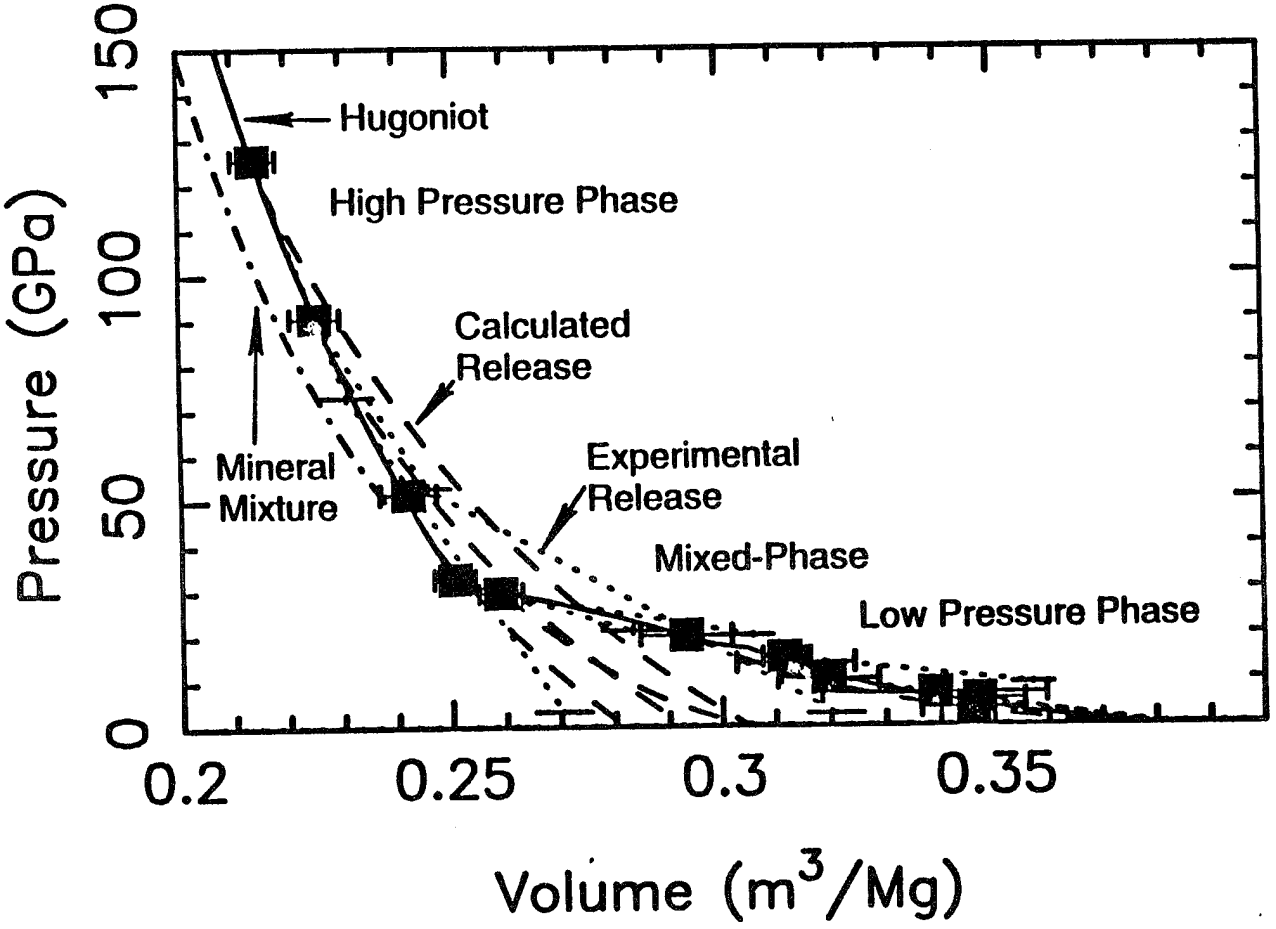

Figure 5-2. Calculated Hugoniot and release adiabats for calcareous shale, compared with the experimental data.

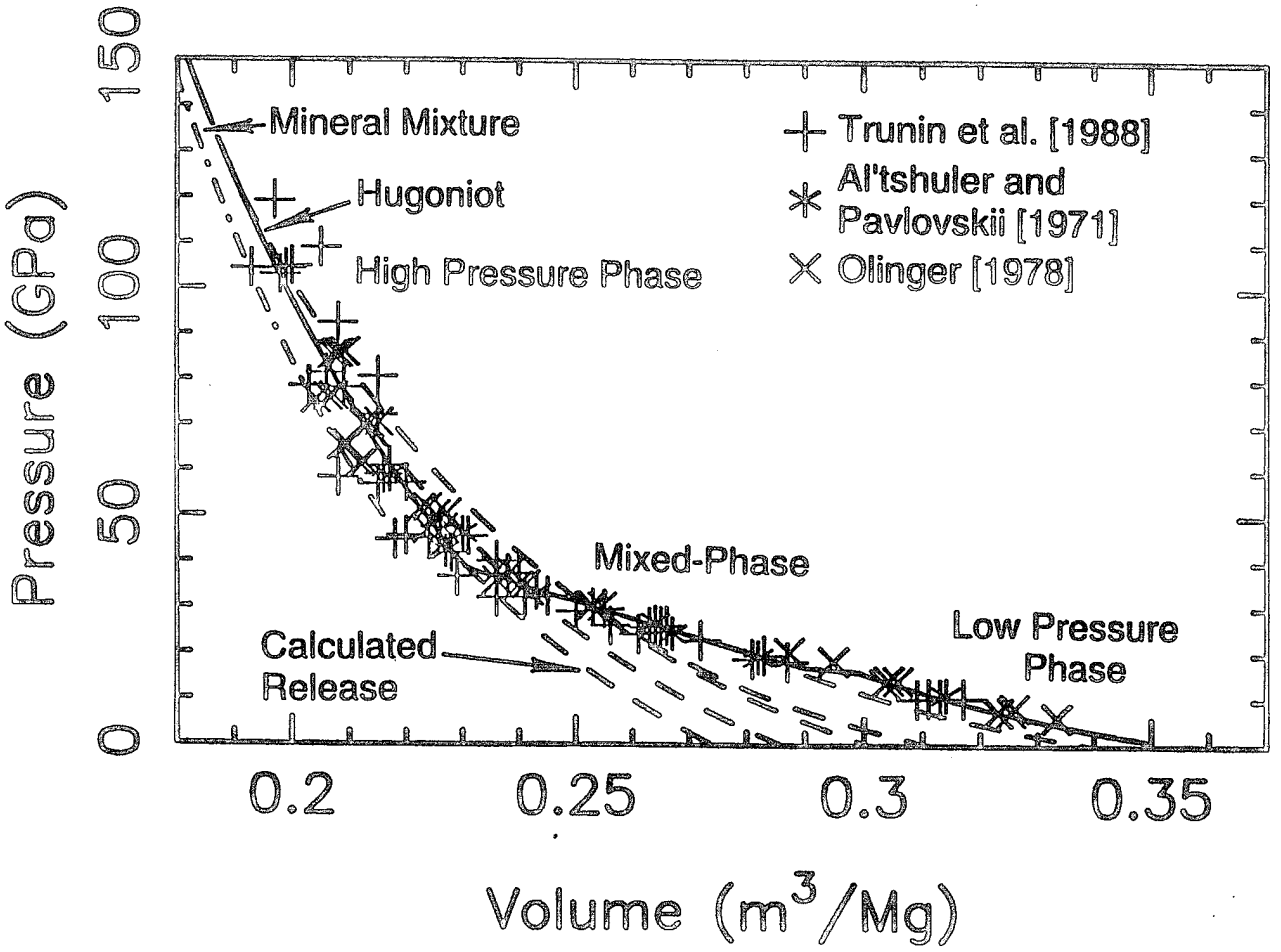

Figure 5-3. Calculated Hugoniot and release adiabats for carbonate-poor shale, compared with the experimental data.

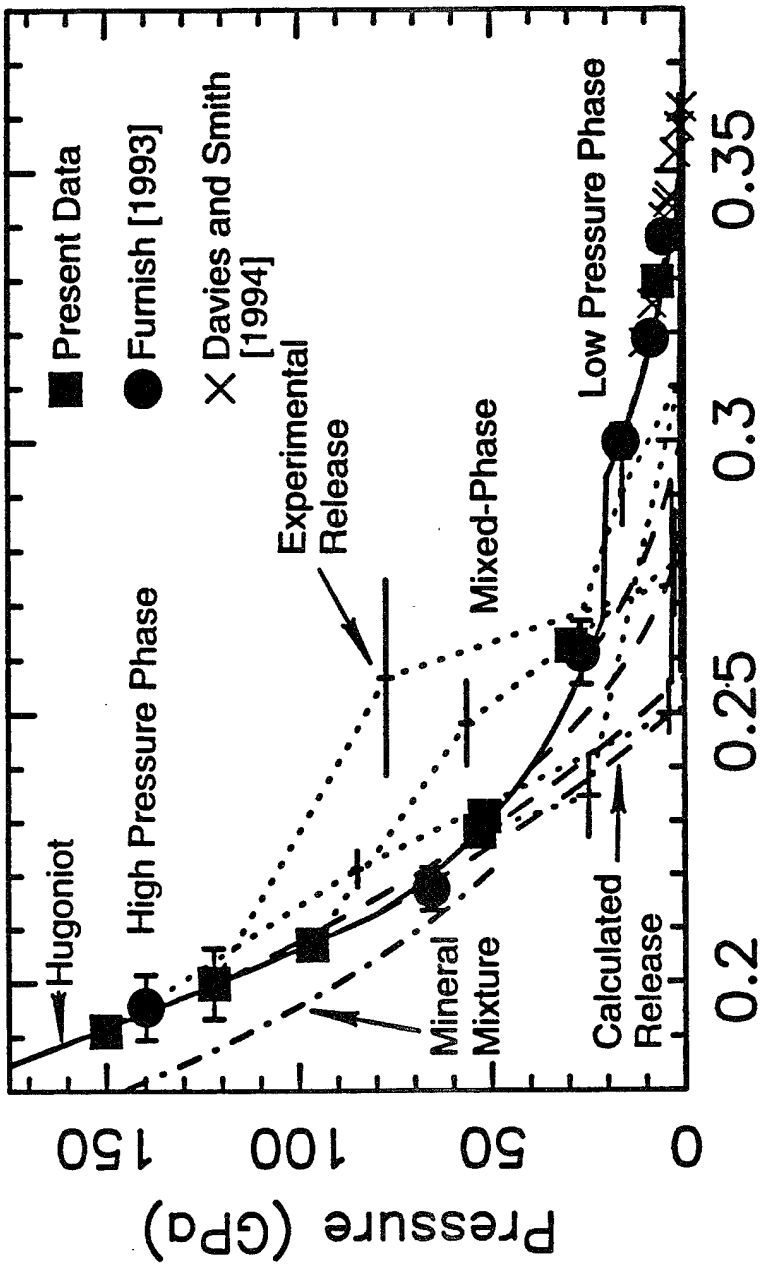

Figure 5-4. Calculated Hugoniot and release adiabats for slate, compared with the experimental data.

principle of volume conservation under mechanical mixing and the greater density of the less water-rich phyllosilicates. The presence of zeolitic water, as was found in the calcareous shale studied here, has an important effect, as it implies the present of very open mineral structures and thus low density. These open structure minerals also are very compressible, so that the whole rock bulk modulus is decreased markedly, at least in the low pressure phase. Surprisingly, the bulk modulus of the low pressure phase of kaolinite, and presumably other clays, is very similar to that of muscovite (and, presumably, other micas). Thus, the primary effect of water content on the bulk modulus is seen only when there is a large zeolitic water content.

The effects of the clay/mica ratio on the densities of the high pressure phases is less important, since the clays seem to undergo a phase transformation, while the micas apparently do not. The content of quartz and other nonhydrous minerals has the most pronounced effect on the bulk modulus of the high pressure phase. Most of these minerals undergo transformation to high pressure phases with large densities and large bulk moduli, so that the corresponding rock high pressure phase will be relatively dense, as seen in the data for the carbonate-poor shale, which appears from the chemical analysis to have significant abundances of plagioclase feldspar and pyroxene.

5.3 RELEASE ADIABATS.

Figures 5-1, 5-2, and 5-4 also present the experimental *P-V* release adiabat points obtained as described earlier. In all cases, the release adiabats from the high pressure region of the Hugoniot parallel the *P-V* Hugoniot at high pressures, with deviation to larger volumes at lower pressures. Release from the mixed-phase regions seems generally to result in large volume increases probably related to reversion to the low pressure phase. Both kaolinite and calcareous shale show large volume increases upon release, especially in the mixed-phase region, similar to the carbonate rocks and minerals [Vizgirda and Ahrens, 1982; Anderson and Ahrens, 1995]. The large volume increases at low pressures strongly suggest that the high pressure phases of these materials revert to the low pressure phase or to some other large-volume phase upon release. The release data for slate are somewhat ambiguous, showing either release paths which parallel the Hugoniot at high pressures, or which show large volume increases at high pressures. Because thermodynamically possible release adiabats should be straight or concave upward in the figure, we suggest that the data showing the large volume increases are in error.

The experimental release points can be used to check the validity of our equations of state. The points shown are actually lower limits on V, since the straight-line approximation of Lyzenga and Ahrens [1978] produces the lower extremum of thermodynamically allowable volume increase upon adiabatic release with no phase change. For a rigorous comparison, one would need to calculate the particle velocity increase for a test release path using the Riemann integral and compare that to the observed particle velocity increases. However, since the release state particle velocities often have fairly large uncertainties, the straight-line approximation of the release path is sufficient for the present study. The assumption that C_V is constant has the advantage of making the pressure P_r of a point on the release adiabat an analytic function of the release state volume V_r and the original shock pressure P_H:

$$P_r = P_{Sr} + (P_H - P_S)(V_H/V_r)^{n-1} \exp\left[\int_{V_r}^{V_H} (\gamma/V)dV\right] \tag{5.4}$$

Figures 5-1--5-4 show these release adiabats, calculated under the assumption that the high pressure phase is "frozen in" at the shock state mass fraction by kinetics. Reversion of the high pressure phase to some other lower density phase is manifested in the figures by experimental release paths at lower pressures that are shallower than the calculated paths. This phenomenon is significant for both kaolinite and shale. However, the higher pressure data generally show good agreement with the calculated release adiabats.

5.4 IRREVERSIBLE HEATING AND ENERGY DEPOSITION.

One important use of calculated release adiabats is the estimation of the energy deposited irreversibly in the rock due to hysteresis in the shock-release path. In terms of the internal energy characteristic of the shock wave, the fraction f' of the energy not recovered, and therefore irreversibly deposited as heat, is given by

$$f' = 1 - \frac{E_r}{E_H} \tag{5.5}$$

where

$$E_r = -\int_{V_H}^{V_H} P_{ad} dV + \sum \Delta E \tag{5.6}$$

where ΔE indicates the energy of transformation of any phase changes, at the conditions under which the phase changes take place, and the subscript *ad* refers to an adiabatic path, which is isentropic for any given single phase.

Figure 5-5 summarizes the values of f' for the shales and slate considered in this study, using the calculated release adiabats shown in Figures 5-2--5-4. Because of the tendency for the real release adiabats to expand to larger volumes at low pressures, these curves give erroneously high values of f'. The exception is for slate, which seems to behave as if the high pressure phase persists to low pressure upon release.

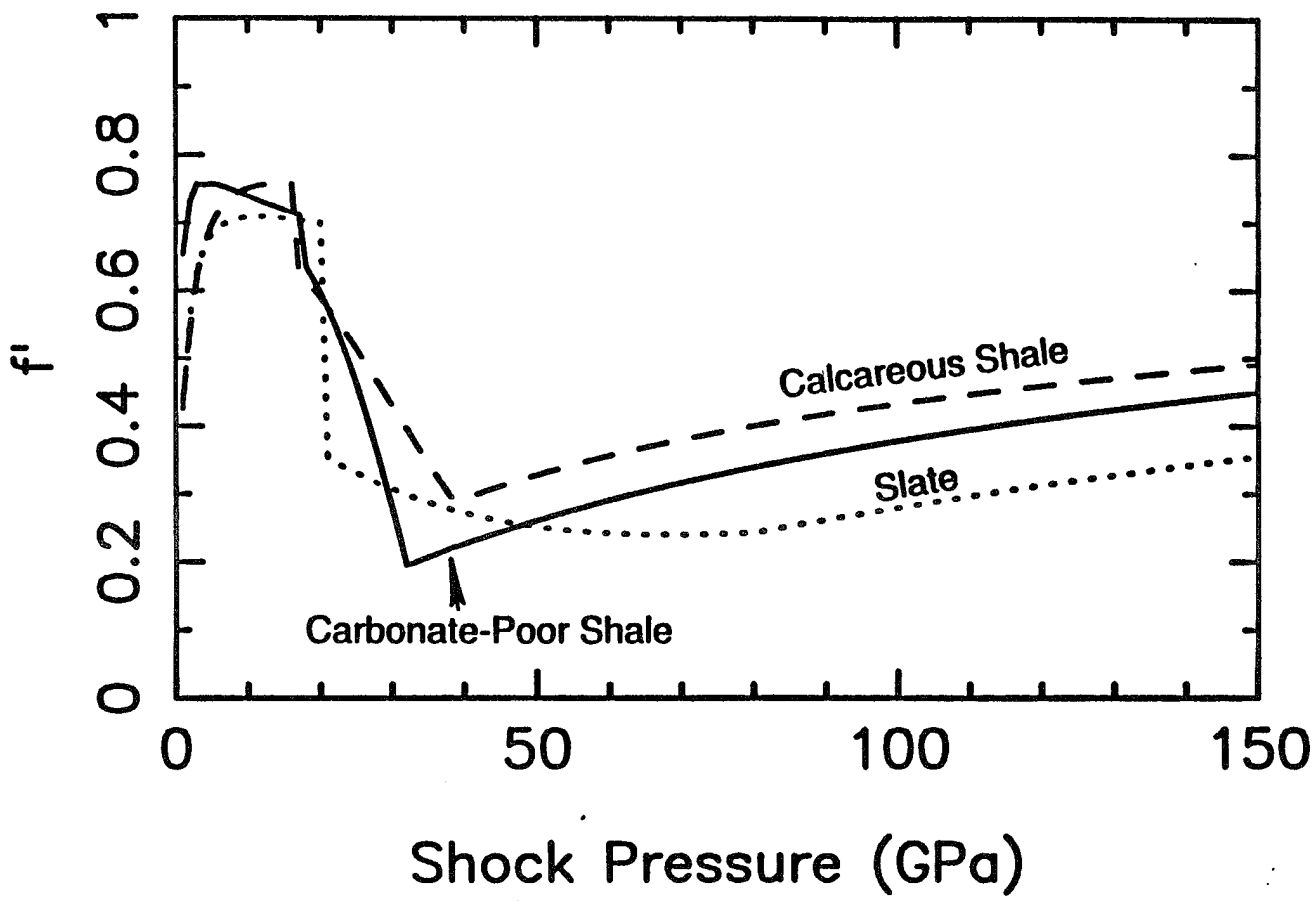

Figure 5-5. Fraction f' of Hugoniot internal energy irreversibly deposited in slate and shale, calculated assuming retention of the high pressure phase upon release. Actual energy deposition will be smaller.

Table 5-1. Equation of state parameters and mixed phase regime Arrhenius equation paramters for kaolinite, shales, and slate.

Material	ρ_0 (Mg/m^3)	K_{S0} (GPa)	K'	γ_0	n	E_{tr} (MJ/kg)	C_V (J/molK)	A	E_a (kJ/mol)	P_{tr}^* (GPa)
Kaolinite:										
(Low P)	2.594	49.4	2.36	1	1	---	1642	---	---	12
(High P)	3.359	157	4	1	1	.5	1642	8	30.5	
Shale:										
Calcareous:										
(Low P)	2.615	30.9	8.15	0.73	1.52	---	1396	---	---	18
(High P)	3.659	265	3.14	1.2	1.49	0.42	1396	58	28.6	
Carbonate-Poor:										
(Low P)	2.813	61.1	4.52	0.79	1.73	---	1159	---	---	17
(High P)	3.740	184	3.24	0.93	1.92	0.62	1159	7.8	15.8	
Slate:										
(Low P)	2.823	50.5	8.00	0.71	1.65	---	1225	---	---	21
(High P)	4.110	432	1.99	0.83	1.8	0.36	1225	1.34	5.26	

*Phase boundary pressure

SECTION 6
REFERENCES

Ahrens, T. J., Equation of state of iron sulfide and constraints on the sulfur content of the earth, J. Geophys. Res., 84, 985-998, 1979.

Ahrens, T. J., Shock wave techniques for geophysics and planetary physics, in Methods of Experimental Physics, vol. 24, Part A, edited by C. G. Sammis and T. L. Henyey, pp. 185-235, Academic Press, San Diego, Calif., 1987.

Al'tshuler, L. V., and M. N. Pavlovskii, Response of clay and clay shale to heavy dynamic loading, J. Appl. Mech. Tech. Phys., 1, 161-165, 1971.

Anderson, W. W., and T. J. Ahrens, Equations of state of sandstone and limestone, in preparation, 1995.

Davies, F. W., and E. A. Smith, High Pressure Equation of State Investigation of Rock, Defense Nuclear Agency Tech. Rept. DNA-TR-94-1, 1994.

Furnish, M. D., Memo to Audrey Martinez, April 20, 1993.

Kikuchi, M., Y. Syono, and B. Velde, Shock wave effects on kaolinite and other clays, Am. Mineral., 78, 904-910, 1993.

Lyzenga, G. A., and T. J. Ahrens, The relation between the shock-induced free surface velocity and the post-shock specific volume of solids., J. Appl. Phys., 49, 201-204, 1978.

Olinger, B. W., Dynamic properties of Devonian shales, in Evaluation of Methods for Stimulation and Characterization of Eastern Gas Shales, Los Alamos National Laboratory, LA-7094-PR, compiled by W. J. Carter and N. E. Vanderborgh, pp. 1-10, 1978.

Robie, R. A., B. S. Hemingway, and J. R. Fisher, Thermodynamic properties of minerals and related substances at 298.15 K and 1 bar (10^5 pascals) pressure and at higher temperatures, U. S. Geol. Surv. Bull. 1452, 1978.

Sekine, T., A. M. Rubin, and T. J. Ahrens, Shock wave equation of state of muscovite, J. Geophys. Res., 96, 19675-19680, 1991.

Trunin, R. F., G. V. Simakov, I. P. Dudoladov, G. S. Telegin, and I. P. Trusov, Rock compressibility in shock waves, Izv. Earth Physics (Engl. Trans.), 24(1), 38-42, 1988.

Vizgirda, J., and T. J. Ahrens, Shock compression of aragonite and implications for the equation of states of carbonates, J. Geophys. Res., 87, 4747-4758, 1978.

DISTRIBUTION LIST

DNA-TR-95-32

DEPARTMENT OF DEFENSE

DEFENSE INTELLIGENCE AGENCY
ATTN: DT-1

DEFENSE NUCLEAR AGENCY
ATTN: DFSP
ATTN: DFTD D LINGER
ATTN: SPWE
ATTN: SPWE E TREMBA
2 CY ATTN: SSTL
ATTN: TDTV F RENSVOLD

DEFENSE TECHNICAL INFORMATION CENTER
ATTN: DTIC/OCP

FIELD COMMAND DEFENSE NUCLEAR AGENCY
ATTN: FCTN B HARRIS-WEST
ATTN: NVTV

FIELD COMMAND DEFENSE NUCLEAR AGENCY
ATTN: FCTT-T B RISTVET
ATTN: FCTT-T E RINEHART
ATTN: FCTT DR BALADI
ATTN: FCTT J HUGHES
ATTN: FCTTS J LEVERETTE
ATTN: FCTTS LT COL LEONARD
ATTN: FCTTS DR REINKE
ATTN: FCTTS P THOMPSON

DEPARTMENT OF THE ARMY

U S ARMY ENGR WATERWAYS EXPER STATION
ATTN: E JACKSON CEWES-SD-R
ATTN: J ZELASKO CEWES-SD-R

DEPARTMENT OF THE AIR FORCE

PHILLIPS LABORATORY
ATTN: PL/SUL

DEPARTMENT OF ENERGY

EG&G, INC
ATTN: D EILERS

LAWRENCE LIVERMORE NATIONAL LAB
ATTN: DONALD LARSON
ATTN: F HEUZE
ATTN: B DUNLAP
ATTN: LEWIS GLENN
ATTN: J RAMBO
ATTN: J WHITE
ATTN: W C MOSS
ATTN: R WARD
ATTN: TECH LIBRARY

LOS ALAMOS NATIONAL LABORATORY
ATTN: DAVID KING
ATTN: FRED APP
ATTN: T KUNKLE
ATTN: T MCKOWN
ATTN: J FRITZ
ATTN: C MORRIS
2 CY ATTN: REPORT LIBRARY
ATTN: J N JOHNSON
ATTN: THOMAS DEY
ATTN: TOM WEAVER

SANDIA NATIONAL LABORATORIES
ATTN: DIV 9321 W BOYER
ATTN: MIKE FURNISH
2 CY ATTN: TECH LIB 3141

DEPARTMENT OF DEFENSE CONTRACTORS

CALIFORNIA INSTITUTE OF TECHNOLOGY
2 CY ATTN: T J AHRENS
2 CY ATTN: W W ANDERSON
2 CY ATTN: Y ZHAO

DEFENSE GROUP, INC
ATTN: ROBERT POLL

ENSCO INC
ATTN: P FISHER

JAYCOR
ATTN: CYRUS P KNOWLES

KAMAN SCIENCES CORP
ATTN: DASIAC

KAMAN SCIENCES CORPORATION
2 CY ATTN: DASIAC

KTECH CORP
ATTN: E SMITH
ATTN: FRANK DAVIES
ATTN: L LEE

LOGICON R & D ASSOCIATES
ATTN: J RENICK

MAXWELL LABORATORIES INC
ATTN: DR E PETERSON
ATTN: J BAKER
ATTN: J MORRIS
ATTN: P COLEMAN
ATTN: S PEYTON

SCIENCE APPLICATIONS INTL CORP
ATTN: DAN PATCH
ATTN: JACK KLUMP
ATTN: L SCOTT
ATTN: MARTIN FOGEL
ATTN: M MCKAY

SRI INTERNATIONAL
ATTN: DR JIM GRAN
ATTN: MARK GROETHE
ATTN: P DE CARLI

TECH REPS, INC
ATTN: F MCMULLAN
ATTN: R NAEGELI

TERRA TEK, INC
ATTN: W MARTIN

TITAN CORPORATION (THE)
ATTN: A FREDERICKSON
ATTN: S SCHUSTER

DIRECTORY OF OTHER (LIBRARI

MARYLAND UNIVERSITY OF
ATTN: RICHARD DICK